Technical Report 1667
July 1994

Gaussian Mixture Models for Acoustic Interference

James W. Bond
David Stein
James Zeidler
NCCOSC RDT&E Division

Stefen Hui
San Diego State University

Approved for Public Release; Distribution is Unlimited

Table of Contents

Executive Summary 1

Background 1
Introduction 1
Summary of Results 1
Conclusions 1

Characterization of Interference Statistics 1

Introduction 1
Noise Statistics for a Moving Interferer 3
MDA Noise Statistics 6
Summary 10

Figures 12

References 33

Appendix A: Mixture Model Comparison and Estimation

Appendix B: Moving Target Hydrophone Statistics

Executive Summary

Background.

This report and two companion reports have been derived from the chapter on detection theory prepared for the High Gain Initiative (HGI) report. The two companion reports, "Detection Processing for Undersea Surveillance" (Confidential) and "Adaptive Locally Optimum Processing for Interference Suppression from Communication and Undersea Surveillance Signals" focus on detection processing. "Detection Processing for Undersea Surveillance" summarizes the status of detection processing for undersea surveillance at the time of the initiation of the HGI program and deals primarily with adaptive filtering. It summarizes the cumulation of many years of effort in the field by J. Zeidler and others. "Adaptive Locally Optimum Processing for Interference Suppression from Communication and Undersea Surveillance Signals" is the cumulation of work by J. Bond, S. Hui, D. Stein, and others on adaptive locally optimum processing for interference suppression and of V. Broman on target tracking. This report summarizes the results of statistical analyzes of power variations due to target motion obtained through simulations and actual data power variations collected during a HGI experiment. The analysis involved fitting the power variation data by Gaussian mixture models. This work was primarily accomplished by D. Stein for the HGI program.

Introduction.

Gaussian mixture models, and a particular class of mixture models known as Middleton Class A Noise Models, have been widely investigated to model the acoustic noise generated by distant shipping. In this report, we discuss the use of Gaussian mixture models to describe the noise generated by a nearby ship. The investigation consists of an analysis of selected HGI hydrophone experimental data to determine its statistical characteristics and of simulations of the power variations expected at a hydrophone within the deep sound channel due to the motion of a source relative to the hydrophone.

Summary of Results.

The following results were obtained for three half-hour segments of experimental hydrophone data selected because they exhibited dominant narrowband interference components:

(a) the complex samples generated from the data from one of the segments was better fit by a two-state Gaussian mixture model than by a Gaussian distribution,

(b) the distributions of the complex samples for two of the segments were not significantly different from Gaussian distributions, and

(c) the phase could be modeled as uniform on $(-\pi, \pi]$ and the real and imaginary components of the complex samples modeled as independent for all three segments.

The simulations of power variations due to target motion led to statistics which were better modeled by either a two-state or three-state Gaussian mixture model than by a Gaussian distribution. Often the data was nearly as well fit by a two-state model as by a three-state model. In addition, the two-state models exhibited consistency over a track traversing multiple convergence zones and the model parameters formed two clusters.

Conclusions.

Nearby shipping can sometimes be well modeled by a Gaussian mixture model. The mixture nature of the statistics can be attributed to changing modal interactions due to target motion.

Characterization of Interference Statistics

Introduction.

Information processing for ocean basin surveillance requires the detection of submarine lines in the presence of interference. The interference can be broadband or narrowband, originating from surface ship traffic, marine life, or ocean waves. The optimum detection processing is known when the interference can be well-modeled as stationary Gaussian noise. A number of powerful processing techniques that provide improved detection performance over traditional processing are available when the interference is non-Gaussian. The broadband component of ocean noise is usually

well-modeled by Gaussian noise. The above considerations led us to focus our attention on the analysis of narrowband interference, presumably arising from ships, to determine the time scales over which the statistics can be modeled as stationary and also to determine the likelihood that the narrowband interference is non-Gaussian.

The Atlantic and Pacific ocean basins may each contain several thousand ships, say 3000, at any given time. Suppose that the high gain array forms 100 or more beams, so that possibly 30 to 60 ships are within a horizontal beam. For a matched field beamformer, the interferences of significant level occur at convergence zone ranges from the spatial cell of interest, reducing the number of ships generating significant interference to about one-tenth of the number of ships in the beam. Furthermore, the ships are of different types, having different equipments and from different countries with different electrical systems, so that narrowband lines from only a few ships, if any, would be expected to interfere with the detection of a narrowband signal of interest in a particular beamformer spatial cell. Each of these ship-generated interfering lines would, in general, be expected to arrive with time varying power, because of the variation in propagation conditions. On some occasions, a particularly strong interfering source on another beam may impact performance on the beam being considered. In any case, it is reasonable to suppose that for a high gain array, two different cases are likely to occur; first, no single narrowband interferer dominates the background noise, and second, a few narrowband interferer's dominate the background noise (Heitmeyer, Davis, and Yen, 1985). In the first case, it is reasonable to expect that the background noise will be Gaussian-like. In the second case, it is reasonable to suppose that the background noise will be changing rapidly due to changing propagation conditions to the array from these few dominating sources of the background noise. A reasonable model for this second case is a Gaussian mixture model; mixture models (Titterington, Smith, and Mackov, 1985) are discussed later.

Consider the case of a single dominating interferer and a target of interest as shown in figure 1. The interference arises from a ship whose acoustic energy couples into the deep sound channel and whose location is such that the propagation paths connecting it with the high gain array passes through a submarine of interest. Under these conditions, the signal-to-noise ratio at the output of the beamformer of the high gain array is expected to be quite dynamic. To see why this might be the case, consider a surface ship moving at 15 knots through an area whose cross-section is determined by beam width and by the width of a convergence zone. At 10 convergence zones, roughly 300 nautical miles, the convergence zone would have a width of about 3 miles, while the arc length associated with a 5-degree beam (roughly 1/10 a radian) would be about 30 miles. A merchant ship could pass through the beam-convergent zone area in as little as 12 minutes and as much as 2 hours.

Mohnkern (1989) has studied the effects of interferer motion on Bartlett and Minimum Variance Distortionless Response (MVDR) beamformers for horizontal arrays using plane wave propagation. For Bartlett beamforming, he finds that the time-averaged main lobe response is broadened and under some conditions reduced and that the nulls are blurred. For MVDR beamforming he finds that the main lobe is similarly affected and that moving interferers are associated with multiple-rank submatrices of the spatial cross-spectral matrix. The details depend on the speed of the interferers, array geometry, and the amount of data used to estimate the spatial cross-spectral matrix. In this report, we present simulation results to show the impact of ship motion on received power at a vertical array for selected spatial cells presumed to contain a target of interest.

The motion of the interferers limits the amount of data available that may be used to estimate a spatial cross-spectral matrix to a time interval for which the interference may be modeled as stationary. Unfortunately, this time interval tends to decrease with increasing array size, while the amount of data required to estimate the spatial cross-spatial matrix increases. For an array of n sensors, the maximum likelihood estimate of the spatial cross-spectral matrix requires 2n independent identically distributed data points from each hydrophone so that the expected output signal-to-noise ratio using estimated spatial cross-spectral matrix is not less than one-half that achieved from *a priori* knowledge of the spatial cross-spectral matrix (Reed, Mallett, and Brennan, 1974).

The motion of the interferers causes the interference in the beamformer outputs to be nonstationarity and thus impacts detection processing. Mixture models

have been studied to model nonstationary interference in communications and undersea surveillance (Baker and Gualtierotti, 1986, 1988, to appear; Berry, 1981; Vastola, 1984; Powell and Wilson, 1989). For these models, adaptive locally optimum processing techniques have been developed. The theory and implementation of this processing constitutes the next subsection of this report. Middleton (1966,1967,1977, 1983,1984, 1991) and Middleton and Spaulding (1983, 1986) pioneered these efforts by determining particular classes of mixture models that are derived from statistical models of the source locations of the interference relative to the receiver. In these models, the Middleton Class A, B, and C models, the mixture parameters are related to general statistical properties of the interference sources. Bouvet and Schwartz (1988, 1989) have fit broadband ocean noise data with the Middleton Class A noise model. These efforts have involved fitting time domain noise data by a Gaussian mixture model. In this report, we extended these efforts by investigating the suitability of modeling narrowband ocean noise data in real-time in the frequency domain by Gaussian mixture models.

Gaussian mixture models are generalizations of Middleton noise models. A Guassian mixture model is defined as follows. Suppose that the indices {1,2,...,M} of the complex samples $z_1, z_2, ..., z_M$ can be partitioned into S disjoint sets $M_1, M_2, ..., M_S$ with the following properties:

$$\text{(a) } \lim_{M\to\infty} \frac{m_k}{M} \text{ exists and equals } p_k > 0$$

for k=1,2, ..., S with m_k the number of the samples with indices from the set $\{1,2,...,M\}$ in M_k;

(b) the real and imaginary components of the interference for the samples contained in the set M_k have identical zero-mean distributions with variance $\frac{1}{2}\sigma_k^2$ for k= 1,2, ..., S with $\sigma_1^2 < \sigma_2^2 < ... < \sigma_S^2$.

If these distributions are zero-mean Gaussian distributions, the mixture model is called a Gaussian mixture model, which is completely described by the parameter set $\{p_1, \sigma_1^2, ..., p_S, \sigma_S^2\}$. The parameter p_k is called the k-th state probability and the parameter σ_k^2 is called the k-th state variance. The probability density function for the normed square of a complex random variable described by a Gaussian mixture model is a sum of exponentials

$$p(|z|^2) = \sum_{k=1}^{S} \frac{p_k}{2\pi\sigma_k^2} e^{-\frac{|z|^2}{2\sigma_k^2}}.$$

Noise Statistics for a Moving Interferer.

In this subsection, we show by simulation that multi-state Gaussian mixture models can be used to describe interferer statistics at the output of a vertical array when the source of the interference is moving relative to the array. For a billboard array, these simulations address the properties of interferers located within the same horizontal beam as the signal of interest. Similar results for interferer statistics at the output of a hydrophone located near the center of the deep sound channel are discussed in appendix B.

The applicability of a Gaussian mixture model to interference generated by multiple moving ships follows readily from the applicability of a Gaussian mixture model for interference generated by a single moving ship. In particular, if $X_1, X_2, ..., X_n$ are independent Gaussian mixture random variables and $Z = X_1 + X_2 + ... + X_n$, then

$$p_Z(x) = (2\pi)^{-\frac{n}{2}} \sum_{k_1=1}^{m_1} \sum_{k_2=1}^{m_2} ... \sum_{k_n=1}^{m_n} p_{1k_1} p_{2k_2} ... p_{nk_n} p(x),$$

where

$$p(x) = \frac{1}{\sqrt{\sigma_{1k_1}^2 + \sigma_{2k_2}^2 + ... + \sigma_{nk_n}^2}} e^{-\frac{x^2}{2(\sigma_{1k_1}^2 + \sigma_{2k_2}^2 + ... + \sigma_{nk_n}^2)}}$$

when

$$p_{X_i}(x) = \frac{1}{\sqrt{2\pi}} \sum_{k_i=1}^{m_i} p_{ik_i} \frac{1}{\sigma_{ik_i}} e^{-\frac{x^2}{2(\sigma_{ik_i}^2)}}$$

with

$$\sum_{k_i}^{m_i} p_{ik_i} = 1 \text{ and } p_{ik_i} > 0, 1 \le k_i \le m_i, \text{ for } 1 \le i \le m.$$

This result follows by induction on n using the fact that the distribution of the sum of two zero-mean independent random variables is the convolution of their distributions with zero mean and variance the sum of their variances.

Simulations were performed to approximate the received power fluctuations from a moving continuous wave (23.804 Hz) interference source. Figure 2 shows the interferer-source-receiving array geometry

for the simulations. The geometry is described by an interfering ship with horizontal range $r(t)$ from a vertical array, an interfering surface ship modeled as a discrete source at depth d_s, and a vertical array consisting of hydrophones at depth d. The interfering ship source is modeled as moving with fixed radial velocity away from the array so that $r(t) = r_0 + vt$, where time starts at 0 and r_0 is the initial distance from interfering ship source to the array and v is its radial velocity. The simulations are designed to examine the properties of the ship interference as received by the hydrophones or for specified vertical beamformer spatial cells. The beamformer spatial cells are chosen to represent cells of interest for the detection of a submerged submarine.

A range invariant normal mode model was used to propagate radiated power from the interferer source to the receiving array. The inputs to this model are ocean depth, water density at the source depth $\rho(d_s)$, water sound speed profile, and sound speed profile in the sediment. The sound speed profiles chosen for the simulations are shown in figures 3 and 4 These sound speed profiles were derived from measurements at the MDA array site, and the depth of the ocean was chosen as 5190 meters, which is the depth at the MDA array.

The modal functions and horizontal wave numbers were calculated using Kraken C (Porter 1992) and the pressure field is calculated using the equation

$$p(r(t), d, d_s) = \frac{1}{\sqrt{8\pi r(t)}} \frac{e^{\frac{i\pi}{4}}}{\rho(d_s)} Z(r(t), d, d_s),$$

where

$$Z(r(t), d, d_s) = \sum_{m=1}^{M} Z_m(d_s) Z_m(d) \frac{1}{\sqrt{k_m}} e^{-ik_m r(t)}$$

with Z_m the $m-th$ modal function, k_m the $m-th$ horizontal wave number, and M the number of modes. In this equation, the pressure field is represented by a complex number. Ninety-eight modes are used for these calculations to capture the significant propagation features.

To study the short-term power fluctuations at the receiving array that occur as an interference source moves, the pressure field was calculated in increments of 0.065 km from a range of 10 km to a range of 876 km. The range increments correspond to the distance a ship with a radial velocity of 5 meters/second (10 knots) traverses in 13 seconds. The receiving array was modeled as consisting of 200 hydrophones, one every 10 meters, extending from a depth of 10 meters to a depth of 2000 meters. The length of the vertical array corresponds to the length of the MDA array.

The received pressures from the moving interference source at 10 meters depth were beamformed by a Bartlett beamformer to characterize the interferer power fluctuations at the output of the beamformer for a moving interferer. A beamformer spatial cell is characterized by the depth of the cell and its range from the vertical array of hydrophones. Results were obtained for four spatial cells at a depth of 100 meters and ranges of 434, 450, 464, and 470 kilometers. These cells are located between convergence zones 7 and 8 at approximately 434 and 496 kilometers. For each cell, the interference power was calculated as

$$10\log_{10}\left(\left|\frac{\vec{v}_r \bullet \vec{v}_0^*}{\vec{v}_0 \bullet \vec{v}_0^*}\right|^2\right)$$

with $\vec{v}_0$ the steering vector for the spatial cell and $\vec{v}_r$ the steering vector for the interferer at range r and depth l0 meters. In particular,

$$\vec{v}_0 = (p(r(t), d_1, d_s), p(r(t), d_2, d_s), ..., p(r(t), d_{200}, d_s)$$

and

$$\vec{v}_r = (p(r(t), d_1, d_t), p(r(t), d_2, d_t), ..., p(r(t), d_{200}, d_t)$$

with

$d_k = 10 + 10(k-1)$ meters for $k = 1, 2, ..., 200$

$d_s = 10$ meters, and

$d_t = 100$ meters.

The Bartlett beamformer results are presented in figures 5a, b, c, and d. Beam patterns with distinct peaks at roughly convergence zone spacing (figures 5a, b, and c) occurred if the range of the cell was within 30 kilometers of a convergence zone, while a more complicated pattern, as shown in figure 5d, was produced for other cells.

The observed power at the hydrophone level and at the output of a Bartlett beamformer attributable to a moving interferer is likely to be nonstationary on a timescale greater than the time required by the source to move about 10 kilometers (one-sixth of a convergence zone). The power may vary by more

than 20 dB over half-hour segments. The periods of the oscillation are variable and depend upon the range of the interferer from the array, the position of the ship relative to convergence zones, and the array configuration. Note that figure 5 presents the power fluctuations due to a single moving source. For real data, the noise power fluctuations would probably be reduced by the presence of background noise. As a result, the dynamic range of the noise and, in particular, the ratio of high-state variance to low-state variance for a Gaussian mixture model depends on the interference-to-background noise ratio. It follows that the dynamic range of actual beamformed data would be less than the estimates obtained from our simulation results for a vertical array.

The predicted beamformed interferer power levels from the moving interferer source at a depth of 10 meters were also used to assess as a function of time whether the power levels could better be described as arising from a one-state or two-state Gaussian mixture model. (We extend the use of the mixture model terminology to include a one-state Gaussian mixture model, by which we mean a Rayleigh distribution.) To simulate a Rayleigh channel, the amplitudes were multiplied by independent unit variance complex Gaussian random variables. In particular, if $\{A_1, A_2, ..., A_n\}$ is a set of amplitudes , the data subject to statistical analysis were $\{z_1 = A_1 c_1, z_2 = A_2 c_2, ..., z_n = A_n c_n\}$, where $c_1, c_2, ..., c_n$ are independent complex random variables with a zero-mean unit variance circular Gaussian distribution. As a result, the data are locally circular Gaussian and the resulting assessment determines if the amplitude fluctuations are best captured by a single-state or a multiple-state Gaussian mixture model.

Statistical analysis was performed for four spatial cells as the source moved from 350 to 450 kilometers from the array. Similar results for a source moving away from a hydrophone are presented in appendix B. Models were fitted using the Expectation and Maximize (EM) algorithm (Zabin and Poor, 1989, 1990, 1991; Powell and Wilson, 1989), as described in appendix A, to 128 successive beamformer amplitudes with 50% overlap. The amplitudes were multiplied by independent unit variance complex Gaussian random variables to emulate complex samples. The results of the statistical analysis are presented in figures 6 through 9 for spatial cells at a depth of 100 meters and ranges from the array of 434, 450, 464, and 470 kilometers, respectively. The abscissa is the horizontal distance between the vertical array and the first point of each of the data sets. Figures 6a through 9a present the significance levels of the Kendall-Mann tau test for the random variable 128 sample average of norms squared and the Kolmogorov-Smirnov two-sample tests for stationarity by comparing the distribution of the first half of the samples with the distribution of the second half of the samples; figures 6b through 9b show the significance levels of the Kolmogorov-Smirnov one-sample test for the one-state and two-state Gaussian mixture model distribution (see appendix A for a description of the statistical tests). Figures 6 through 9 show the estimates of the high-state to low-state variance and the low-state probability of the best two-state fit of the data obtained using the EM algorithm. Figure 10 shows the joint probability density function of the low-state probability and the ratio of the high-state to low-state variance for the two-state mixture model parameters that best describe the interference data for the four spatial cells.

The multistate nature of the frequency domain beamformed interference is implied by the low significance levels shown in figures 6b through 9b of the test for the one-state Gaussian mixture model (significance levels were truncated at 10^{-3}, and in some plots all values were at or below this value). Also, the significance levels of the two-state Gaussian mixture model distribution are generally lower for the beamformed data than for the hydrophone data. This can be verified by comparing figures 6 through 9 with figure B-3 of appendix B.

The dynamic range of the frequency domain beamformed data is generally higher than for the hydrophone data. Generally speaking, only two successive 10-kilometer estimates are described by nearly the same mixture model, indicating that the interference should be modeled by a given Gaussian mixture model for periods of time not exceeding the time for the interferer to move to or away from the receiving array by more than 30 kilometers.

The Kolmogorov-Smirnov one-sample test significant levels tended to decrease as the variance ratios increased. See appendix A for a description of this and other statistical tests used to evaluate model distributions. The absolute values of the correlations are 0.25, 0.20, 0.38, and 0.72 for the data in figures 11, 12, 13, and 14, respectively. Inspection of the

cumulative distributions suggests that often a three or more state Gaussian mixture model would fit the data segments having large dynamic ranges better than a two-state model. Examples of such distributions are shown later in this subsection. This observation led us to investigate the applicability of three-state mixture models to the simulated moving interferer data.

Figures 11 and 12 present histograms of the significant levels of one-state, two-state, and three-state models compared to the empirical distributions of the data for the Chi-squared test and the Kolmogorov-Smirnov one-sample test, respectively. Figure 13 presents a histogram of the average differences (L2 norms) between the one-state model and the two-state model, the one-state model and the three-state model, and the two-state model and the three-state model. These histograms reveal that the two-state and three-state models often lead to distributions that differ.

Figures 14 through 18 show five examples of the one-state model, two-state model, and three-state model cumulative probability functions compared to the empirical cumulative probability function for the beamformed data. Figures 14 and 15 illustrate cases when the two-state model fit and three-state model fit to the beamformed data are nearly the same and quite different, respectively. The three-state fit is clearly better than the two-state fit for the data presented in figure 15. Figure 16 shows a worse case fit for the one-state model with the lowest significance level for the Chi-squared test. Note that the tail of empirical distribution falls off much slower than the tail of the one-state fit leading to a high Chi-squared test score and correspondingly low significance level. This distribution is well fit by the three-state model and not well fit by a two-state model. Figure 17 shows a worst case fit for the two-state model according to the Chi-squared test; the three-state fit, which is nearly the same as the two-state fit, is also poor. Figure 17 illustrates a distribution that requires more than three states to be well fit. Figure 18 presents the data for a worst case three-state fit according to the Kolmogorov-Smirnov one-sample test. These examples illustrate the great variety of cases that arose fitting the frequency domain beamformed interference levels from a moving ship.

Figure 19 summarizes the probabilities of occurrence of the three-state model parameters p_L, p_M, p_H, $\frac{\sigma_M^2}{\sigma_L^2}, \frac{\sigma_H^2}{\sigma_L^2}$ obtained by using the EM algorithm for the beamformed data. The surprising result is the high percentage of cases in which the best three-state model probability was between 0.4 and 0.6 as shown in figure 19b. Analysis was conducted to cluster the parameter data for the three-state model. The analysis did not reveal the strong clustering of model parameters for the three-state models as exhibited for the parameters of the two-state models. The best defined cluster (12 %) of joint model parameters occurred for low state probability between 0.1 and 0.2, the middle-state probability between 0.36 and 0.55, the high-state to low-state variance between 64 and 2048 , and the high-state to middle-state variance between 4 and 64 . The next best defined cluster (9 %) of joint model parameters occurred for low-state probability between 0.2 and 0.3, the middle-state probability between 0.3 and 0.6, the high-state to low-state variance between 64 and 1028, and the high-state to middle-state variance between 4 and 32.

The simulations suggest that a multi-state Gaussian mixture model may better characterize the interferer power fluctuations over a half hour than does a one-state model. The simulations for a hydrophone (described in appendix B) and a vertical array indicate that mixture models should apply to both, with the ratio of high-state to low-state variance greater for the beamformed output interference power than for the hydrophone output interference power.

MDA Noise Statistics.

Frequency domain statistics were obtained by spectrally processing selected segments of hydrophone data collected during the MDA experiment. Three half-hour segments of hydrophone data for specific Fourier transform frequency bins containing dominant narrowband lines, presumably ship-generated, were selected for detailed analysis. In addition, the data were surveyed for all frequencies to establish the frequency of occurrence of bins exhibiting two-state Gaussian mixture characteristics and to determine the correlation of statistics between adjacent frequency bins. Hydrophone data were used for the analysis because these data are easier to survey than beamformed data for the presence of dominant narrowband interference.

The selected hydrophone data were Fourier transformed with a frequency resolution that represents a reasonable choice for the resolution of a matched field beamformer. The results obtained for hydrophone data should be relevant because matched field beamforming is a linear process. In addition, the simulations presented in the previous subsection and appendix B indicated that Gaussian mixture characteristics, albeit with slightly different mixture parameters, should be observed for hydrophone outputs as well as for the beamformer outputs.

The three half-hour segments of MDA data were collected on day 193 during the hours 0140 to 0740. These segments, hereafter referred to as segments A, B, and C, were selected because their data exhibited high levels of narrowband interference as shown in figures 20, 21, and 22. Segment A spans 0140 to 0210, segment B spans 0440 to 0510, and segment C spans 0710 to 0740 zulu time. Frequency bins with spikes near 24 Hz were analyzed in detail. The bins chosen for segments A, B, and C have frequencies of 23.914, 23.951, and 23.804 Hz , respectively. The interference levels in these bins are presumably dominated by acoustic energy from ships. Note that the large spike seen at 24 Hz in figure 22 is one of the signals generated as part of the MDA experiment.

The likely interferer sources for the selected segments were further characterized by beamforming the hydrophone data by using a modal beamformer. This beamformer processes the vertical component of the incoming wavefront as described in the previous subsection (Bartlett beamformer) and the horizontal component as a plane wave. Figures 23, 24, and 25 show the sum of mode powers as a function of bearing for segment A at a frequency of 23.914 Hz, for segment B at a frequency of 23.950 Hz, and for segment C at a frequency of 23.804 Hz. These figures indicate a dominant beam and several prominent beamformer side lobes. The side lobes exist because of the hydrophone geometry of the MDA receiving array. Figure 23 indicates a ship on a bearing of -69°, figure 24 a ship on a bearing of 118°, and figure 25 a ship on a bearing of -3°.

The hydrophones chosen were the ones most strongly ensonified by the selected narrowband sources. The chosen hydrophones were 21, 8, and 11, for segments A, B, and C, respectively. The time series data were collected at 150 samples per second and transformed by using a 4096-point fast Fourier transform with 50% overlap and a Hanning window. This transformation has a frequency resolution of 0.036 Hz and results in about 130 complex Fourier coefficients for each frequency for a half-hour of time series data.

Figures 26, 27, and 28 present scatter plots of the real and imaginary components of the complex Fourier coefficients for the selected frequencies of the segment A, B, and C hydrophone data, respectively. The figures indicate that the real and imaginary components of the samples can be treated as uncorrelated random variables. Figures 29 and 30 present histograms of the amplitudes of the complex Fourier coefficients and the phases of the complex sample phases, respectively, for the selected frequency data for segments A, B, and C. It is difficult to conclude from figure 29 whether a given data set is best fit by a one-state or multiple-state Gaussian mixture model. Figure 30 indicates that the phase is better modeled by a uniform distribution than by a single value or several discrete values of phase.

The initial statistical analysis of the frequency domain hydrophone data was structured to determine if the data for the selected frequencies for segments A, B, and C were stationary. The statistical tests, which are described in appendix A, also addressed the suitability of modeling the frequency domain narrowband interference samples by a circular Gaussian distribution. The results of these tests are summarized in table 1.

The results of applying the Kendall-Mann tau tests to A, B, and C segments indicate that sometimes the real and imaginary component Fourier coefficient means and variances for the selected interferer frequency bin seem to contain trends and sometimes not. In general, the results are not conclusive, and only two tests, lack of trends in the means of the real components of the Fourier coefficients of segment A and lack of trends in the means of the imaginary Fourier components of segment C, had high significance levels. Three times the significance levels are below 0.10, indicating trends in the means of the real Fourier coefficients of segment C, variances of the real Fourier coefficients of segment A, and variances of the real coefficients of segment C. All these results are explained by supposing that at times the narrowband interference had a frequency close to that of the center frequency of the Fourier bin for

Table 1. Statistical Test Summary of Suitability of Single State Gaussian Mixture Model for Selected Data

RANDOM VARIABLE	NULL HYPOTHESIS	TEST	Significance Level H_A	H_B	H_C
x y	No shifts in means of distributions	Kendall-Mann Tau	.78 .63	.63 .22	.05 .96
|x| |y|	No shifts in variances of distributions	Kendall-Mann Tau	.06 .52	.59 .63	.09 .11
x y	Distributions for first half samples same as for second half	Kolmogorov-Smirnov two sample	.52 .67	.90 .19	.15 .55
x y x y	Samples have Gaussian distribution Samples have Gaussian distribution	Kolmogorov-Smirnov one sample* CHI-squared test	.63 .48 .37 .10	.79 .61 .04 .05	.41 .74 0** 0**
|z| |z|	Samples exponentially distributed Samples exponentially distributed	Kolmogorov-Smirnov one sample* CHI-squared test	.60 .11	.61 .22	.004 0**
x,y	Sample distributions of real and imaginary components are independent	Kendall-Mann Tau rank correlation test	.24	.66	.61
x,y	Sample distributions of real and imaginary components are the same	Kolmogorov-Smirnov two sample	.32	.01	.17

* Significant levels not adjusted to account for the estimation of parameters
** Significant level less than, 001 are recorded as 0

which the data are being analyzed and as a result slowly changing Fourier transform coefficients .

The Kolmogorov-Smirnov two-sample test was used to test the hypothesis that the distributions of the real and imaginary components of the complex Fourier coefficients were stationary by comparing the distribution of the first half of the samples with the distribution of the second half of the samples. A lack of stationarity is indicated for the distributions of real components of the Fourier coefficients for segment C and for the imaginary components of segment B.

The Kolmogorov-Smirnov test was also used to compare the empirical distributions of the real and imaginary components of the Fourier coefficients with Gaussian distributions, and the distributions of the normed squares of the complex samples with an exponential distributions. The comparisons of the distributions with Gaussian distributions resulted in significance levels between 0.41 and 0.79 without accounting for the estimation of the Gaussian distribution parameters, which would lower the significance levels. Thus, both the real and imaginary components of the Fourier coefficients for all three segments of data are close to Gaussian. The most striking result for the comparison of the complex Fourier coefficients is that the distribution of segment C data is definitely not an exponential distribution of norms squared (significance level 0.004), while segments A and B data had significance levels of 0.60 and 0.61, respectively. This result indicates that segment C might provide an example of a narrowband interferer whose frequency domain samples could be better modeled by a multistate Gaussian mixture model than a one-state Gaussian mixture model.

Consider figure 31 for a suggestive mechanism for the data of segment C being better fit by a multistate mixture model than for a single state. The results presented in figure B-3 of appendix B show that amplitude oscillations consistent with a mixture model may occur in hydrophone data dominated by reception of a narrowband signal from a moving ship because of the interaction between different modes. Figure 31 presents the mode spectrum of the segment B and C data for bearings of 127° and -3°, respectively, the directions from which the most power arrived for the selected frequencies for the three data sets. Note that the modal structure of segment C differs from that of segment B in that there are two peaks in the mode spectrum of segment C and single peaks in the mode spectra of segment B. Thus, segment C is more likely to exhibit modal interference effects than segment B.

Given that the segments were fairly Gaussian-like, and the earlier results that when in doubt the best mixture model is the one with the fewest states, we decided to fit the selected hydrophone frequency domain data with two-state mixture models. An important additional consideration was that the mixture model parameter estimation technique needed to give reasonable results for sample sizes around 130 .

The EM procedure was used to estimate two-state Gaussian mixture parameters for the selected frequency data for segments A, B, and C. In addition, the EM procedure was used to fit the selected frequency data for segment C. Table 2 summarizes the two-state mixture model parameters obtained in this way and table 3 summarizes the three-state mixture model parameters obtained in this way.

Table 2. Two-state Gaussian mixture model parameters for selected hydrophone data.

	Segment A	Segment B	Segment C
p_L	1.00	1.00	0.47
p_H	0.00	0.00	0.53
σ_L^2	97	269	108
σ^2	97	269	327
σ_H^2	0	0	520

The Kolmogorov-Smirnov one-sample test and the Chi-squared test were used to compare the two-state mixture model distributions to the distributions of the data for segment and resulted in significance levels of 0.86 and 0 as compared with 0.004 and 0 for the exponential distribution of norms squared. Thus, the segment C data is better fit by a two-state Gaussian mixture model than a one-state mixture model. The data are slightly better fit, as expected, by a three-state mixture model, as indicated by an increase

Table 3. Three-state Gaussian mixture model parameters for hydrophone data Segment C.

p_L	0.34
p_M	0.61
p_H	0.05
σ_L^2	92
σ_M^2	360
σ_H^2	1998

of the Chi-squared test level of significance to 0.005. However, the Chi-squared test result indicates the segment C data might be better fit by a mixture mode with more than three states. These conclusions are borne out by the distribution shown in figure 32. The one-state model distribution does not fit either tail of the empirical distribution. The two-state and three-state model distributions fit the tails of the empirical distribution better than the one-state model distribution, but neither fits the middle of the empirical distribution very well.

We briefly considered how close the probabilities given in table 3 would be to those with the relationships predicted by a three-state approximation to a Middleton Class A noise model. Toward this end, we found the value of A for which $p_L = e^{-A}$, $p_M = Ae^{-A}$, and $p_H = 1 - e^{-A} - Ae^{-A}$ gives the best least squares fit to the state probabilities presented in table 3. The result is $A \cong .84$ for which $p_L \cong .43$, $p_M \cong .36$, and $p_H \cong .21$. Next, we fixed the low-state variance and the total variance, and minimized the total least squared error as a function of the middle-state variance for the resulting distribution. This leads to $\sigma_L^2 \cong 92$, $\sigma_M^2 \cong 642$, and $\sigma_H^2 \cong 372$. If we impose the additional condition that the middle-state variance is between the other two variances we obtain $\sigma_L^2 \cong 92$ and $\sigma_M^2 = \sigma_H^2 \cong 543$. The best three-state model fit is quite different from a three-state approximation to the Middlleton Class A noise model.

Figure 33 summarizes the salient features of the low-state membership function (low-state probability) for the two-state model best fitting segment C. Figure 33a shows that on two occasions, samples 20 through 46 and samples 98 through 130, all the samples were with high probability in the low state, while the remainder of the time successive samples remain with high probability in the low state for a few states at a time. Observe that the ratios of high-state to low-state variance would decrease if the data were processed after averaging the power over as few as 6 samples. Figure 33b suggests that about 80% of the samples are either assigned with reasonable probability to either the low state or the high state of a two-state model.

Narrowband ship lines are likely to occupy adjacent frequency bins for the frequency resolutions of the Fourier transforms used to obtain the selected frequency data for segments A, B, and C. This feature is of interest, because it allows adjacent frequency bin data to be used to construct a noise model for the interference of the middle bin and in this way to obtain presumably signal-free noise samples. To gain some understanding of how applicable Gaussian mixture models might be to modeling narrowband interference, all frequency bins for segment C data were fit by a two-state model. The results are summarized in figure 34. Of particular interest is that several adjacent bins to that of the selected frequency for segment C, 23.804 Hz, are better fit by a two-state model than a one-state model. The significance levels presented in figure 34b use the Kolmogorov-Smirnov one-sample test with significance levels uncorrected for parameters estimated. In particular, we call the readers attention to the data presented in figures 34c and d. Figure 34 also indicates several other frequency bins for which the interference might better be modeled by a multiple-state model than by a one-state model.

Summary.

The real and imaginary components of the Fourier transforms of distant shipping noise can be modeled by independent Gaussian distributions. Underwater acoustic interference generated by individual ships can be modeled by Gaussian mixture models.

Simulations were conducted to predict received narrowband energy from a moving source by a hydrophone located in the deep sound channel or by a vertical array located in the deep sound channel. These simulations indicated that the interplay between ship movement and propagation mode interaction leads to the received energy being better modeled by a multiple-state Gaussian mixture model than by a

one-state Gaussian mixture model. Usually the interference is well modeled by a two-state or three-state Gaussian mixture model, with rare occurrences of time periods during which the simulated data would be better modeled by a Gaussian mixture model with more than three states.

The EM algorithm was used to obtain the best estimates of the two-state and three-state parameters that best fit the simulated hydrophone, the simulated beamformer output, and the MDA hydrophone output interference data. The distributions obtained by using the EM estimated parameter values were then compared to the empirical distributions. The consistency of the results obtained indicates that the EM algorithm could be used to obtain Gaussian mixture model parameter estimates from real hydrophone or beamformer output data.

The two-state mixture model parameters that best model the simulated beamformer output power levels clustered about two parameter vectors. The analysis shows that two distinct two-state mixture Gaussian power as the ship traverses multiple convergence zones. Three three-state model parameter values did not cluster as much as the parameter values of the two-state models. Given that related mixture models were manifested in both the hydrophone and beamformed simulation data and that MDA hydrophone data were more accessible than MDA hydrophone data processed through a matched field beamformer, we decided to verify the simulation results by analyzing three half-hour segments of MDA hydrophone data. These segments were chosen to contain narrowband data, presumably from a single source. Analysis of the selected segments of data indicated that one of the three was well described by a two-state Gaussian mixture model, while the remaining two exhibited Gaussian statistics. Thus, one of the three selected MDA hydrophone data sets exhibited Gaussian mixture characteristics. The reader should not be concerned that two of three did not exhibit strong mixture characteristics, for the simulations only addressed ship interference for ship ranges from the hydrophone or vertical array for which there would be significant modal interference. Distant ships would not be expected to exhibit such modal interference.

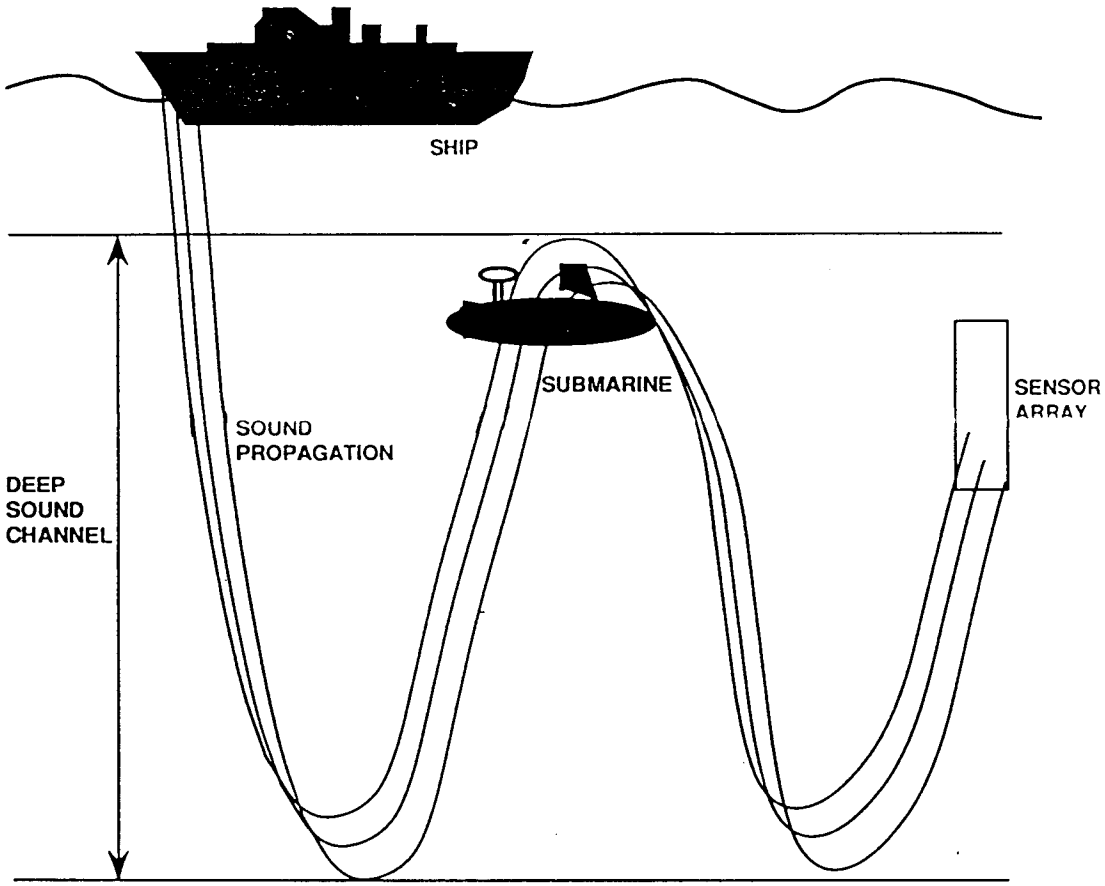

Figure 1. *Single dominant interferer geometry.*

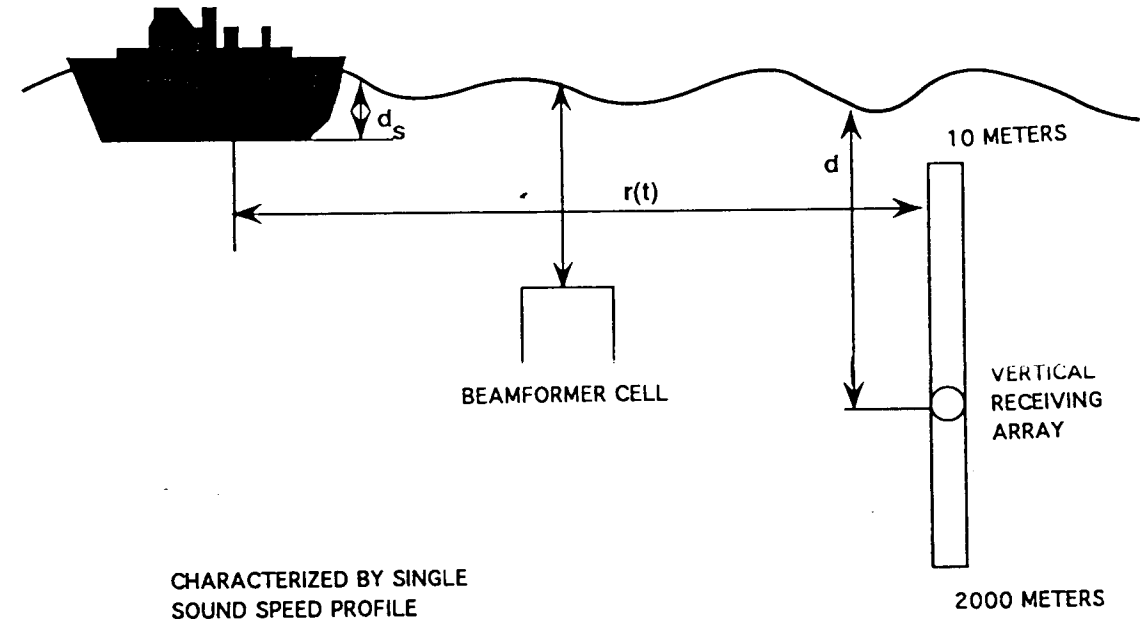

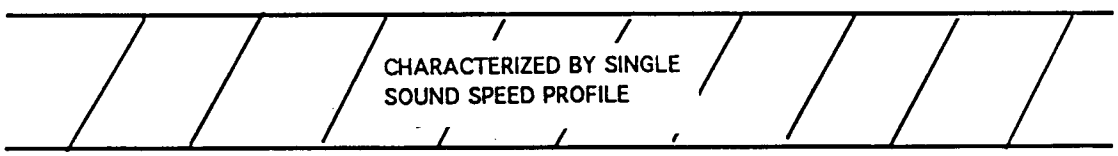

Figure 2. Geometry for moving interferer simulations.

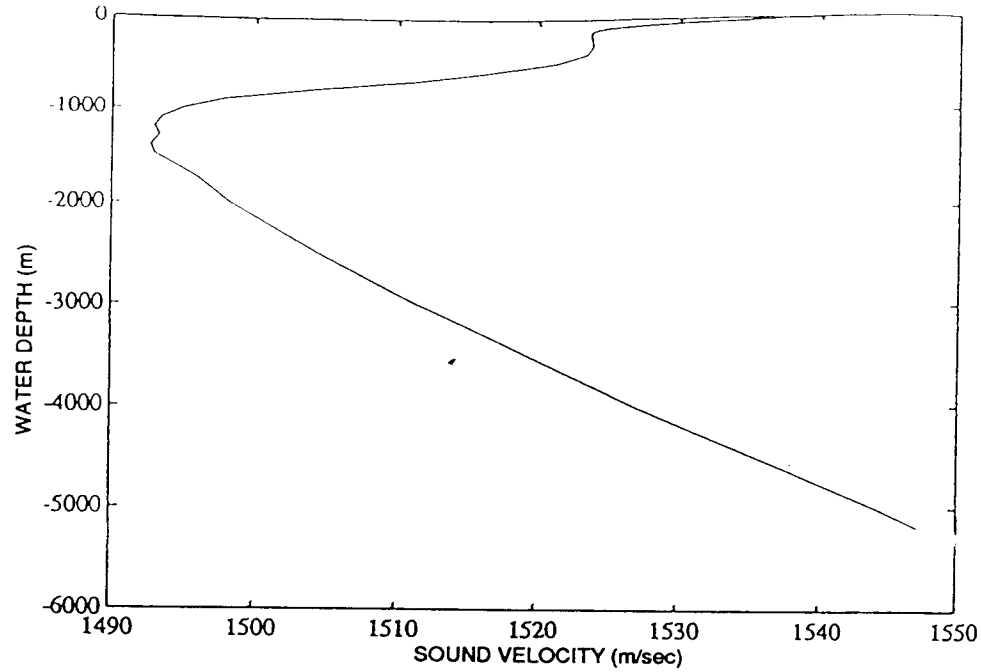

Figure 3. Sound velocity profile for ocean.

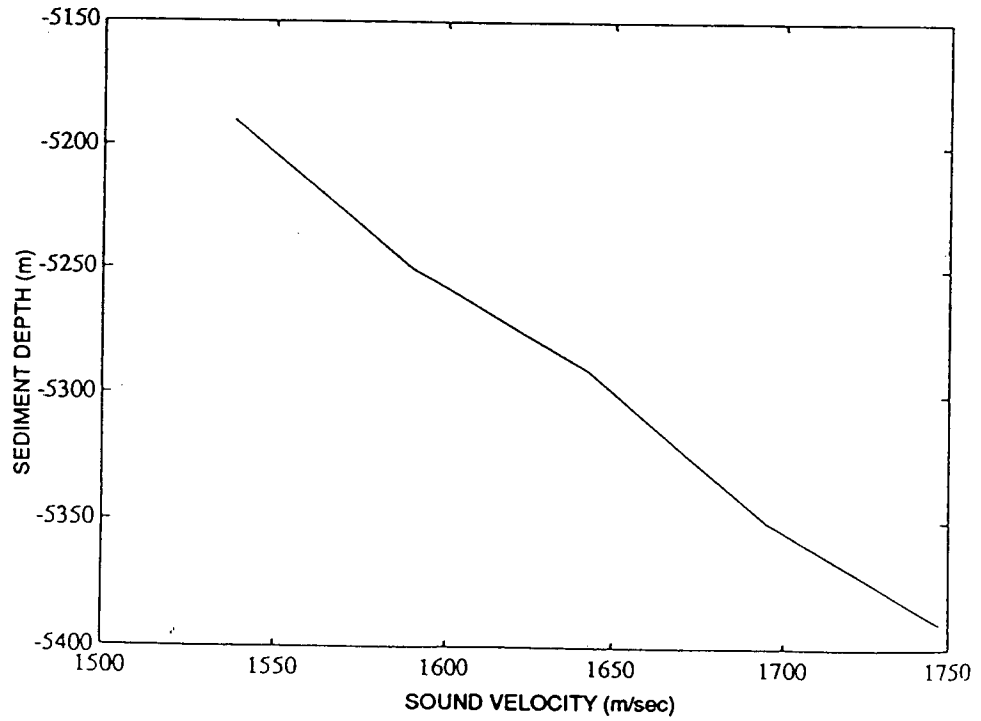

Figure 4. Sound velocity profile for sediment.

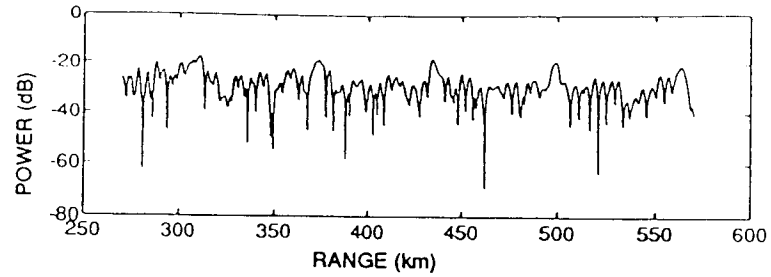

(a) Cell 100 meters deep and at 434 km range.

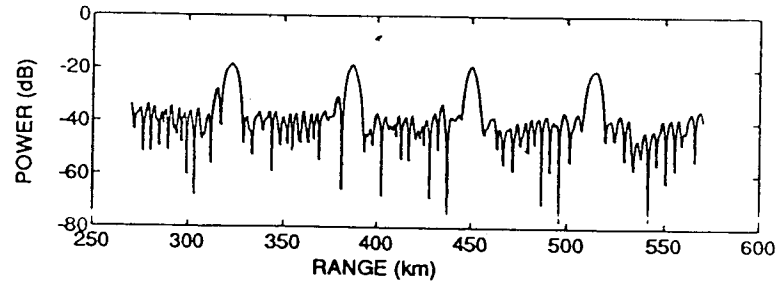

(b) Cell 100 meters deep and at 450 km range.

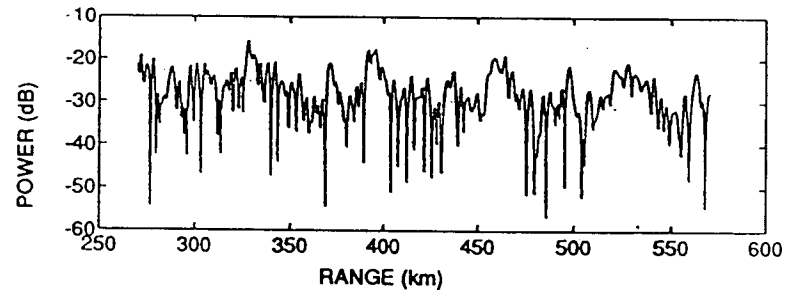

(c) Cell 100 meters deep and at 464 km range.

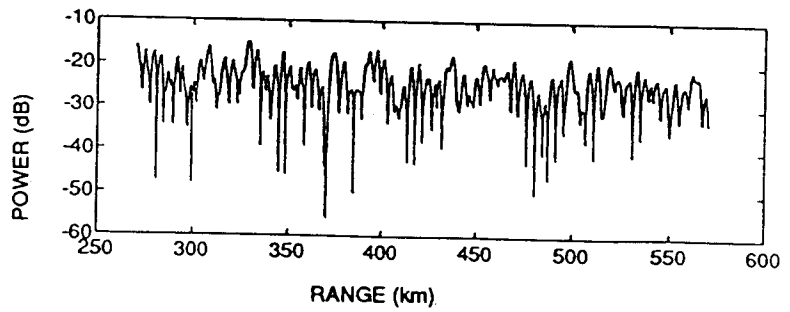

(d) Cell 100 meters deep and at 470 km range.

Figure 5. Vertical array Bartlett beamformer output power.

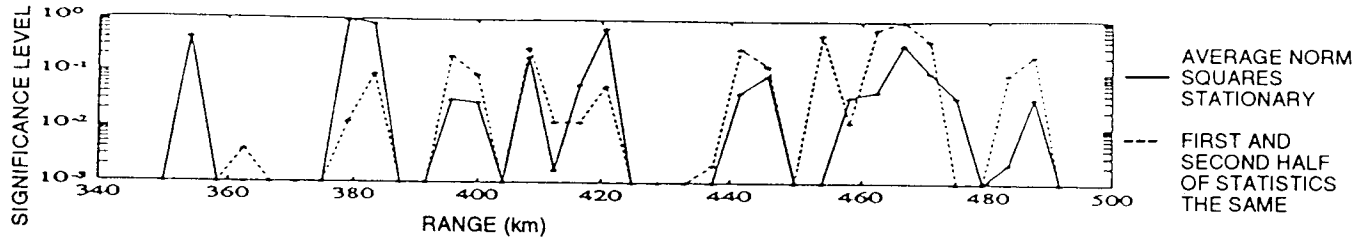

(a) Stationarity of statistics

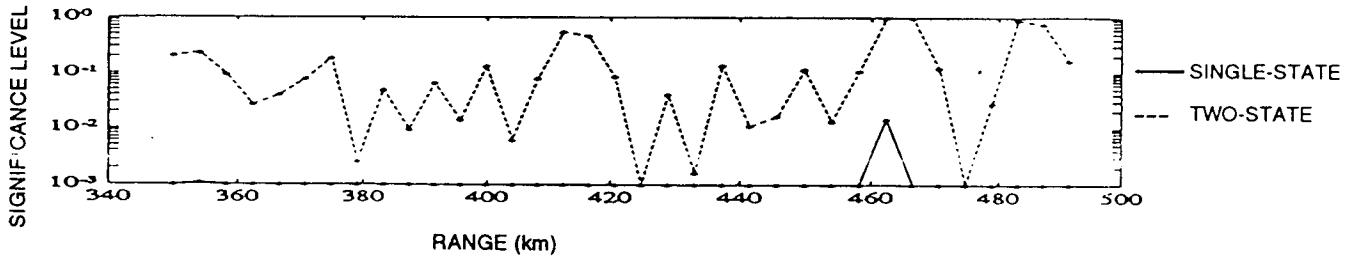

(b) Nature of model

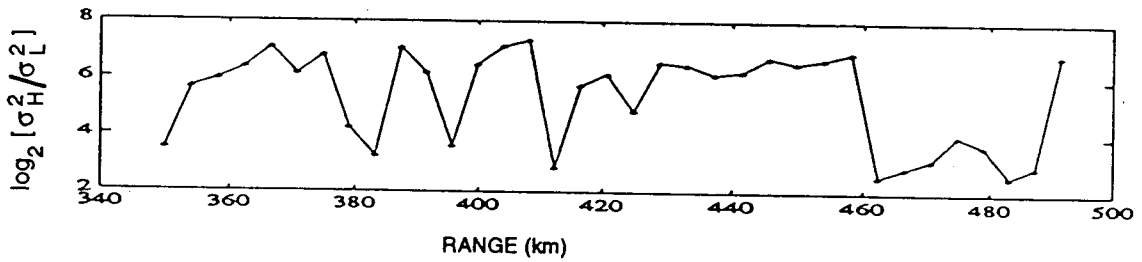

(c) Variance ratio estimates for two-state model

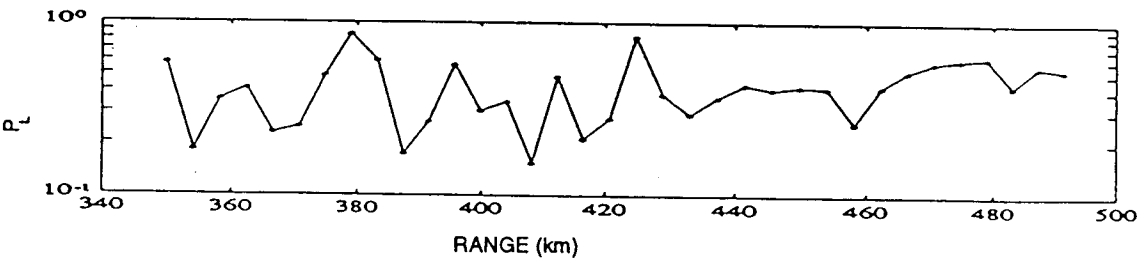

(d) Low-state probability estimates for two-state model

Figure 6. Interferer statistics as a function of range from a moving source and receiving vertical array spatial cell at a depth of 100 meters and a range of 434 kilometers.

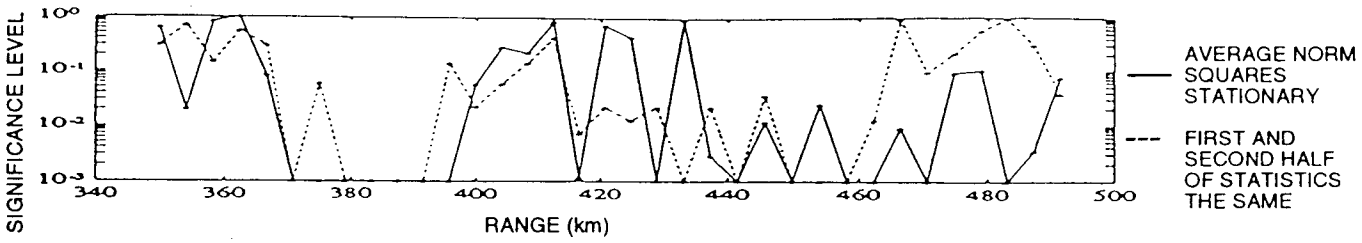

(a) Stationarity of statistics

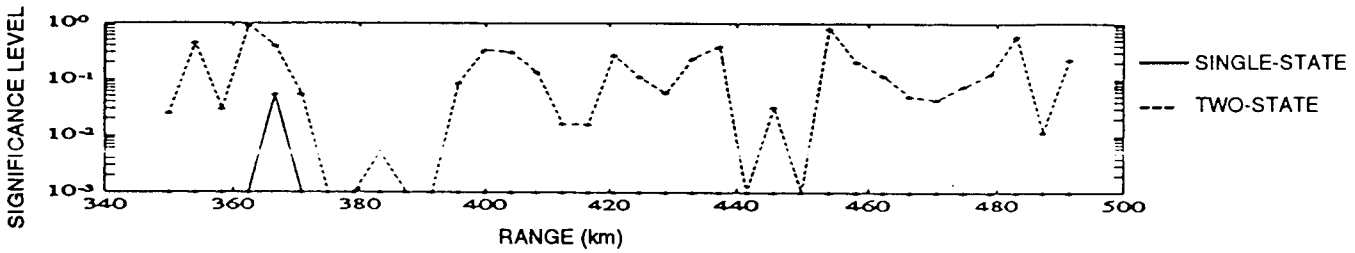

(b) Nature of model

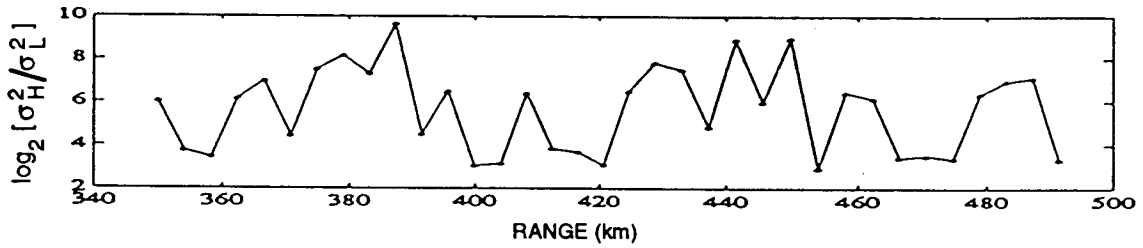

(c) Variance ratio estimates for two-state model

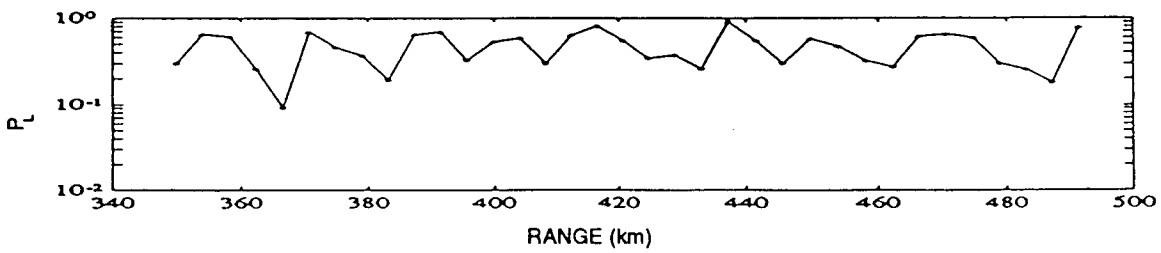

(d) Low-state probability estimates for two-state model

Figure 7. Interferer statistics as a function of range from a moving source and receiving vertical array spatial cell at a depth of 100 meters and a range of 450 kilometers.

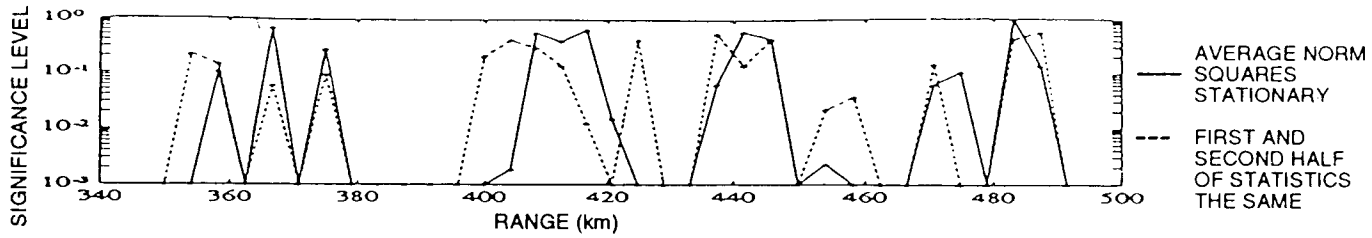

(a) Stationarity of statistics

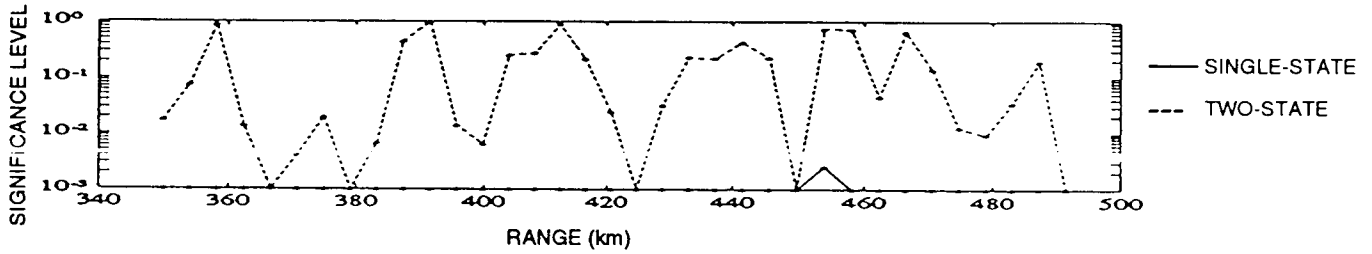

(b) Nature of model

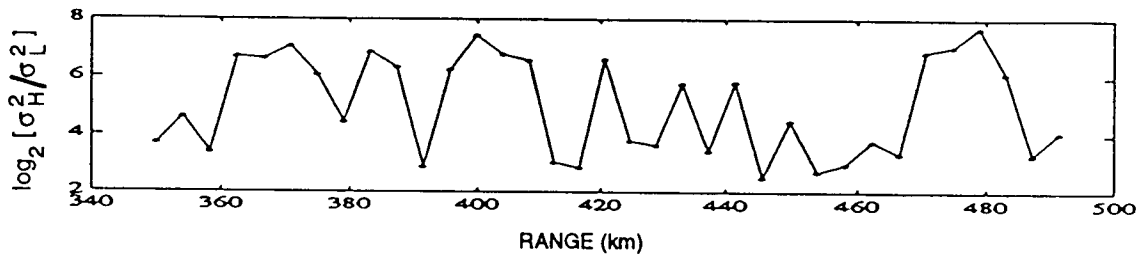

(c) Variance ratio estimates for two-state model

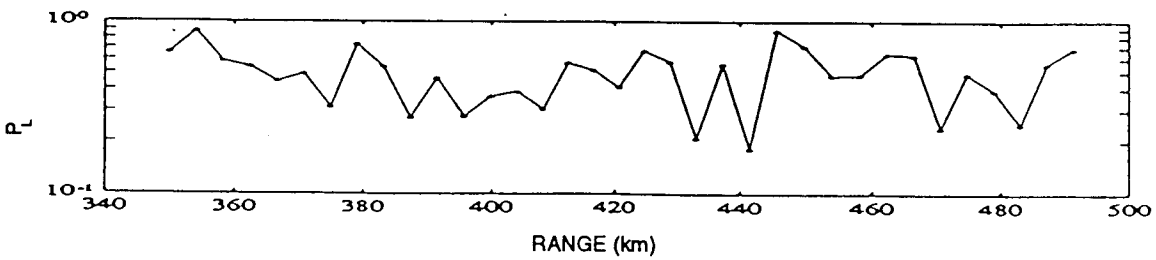

(d) Low-state probability estimates for two-state model

Figure 8. Interferer statistics as a function of range from a moving source and receiving vertical array spatial cell at a depth of 100 meters and a range of 464 kilometers.

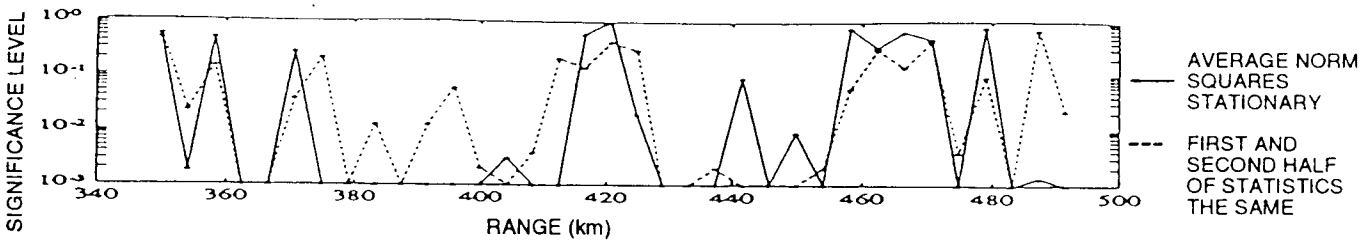

(a) Stationarity of statistics

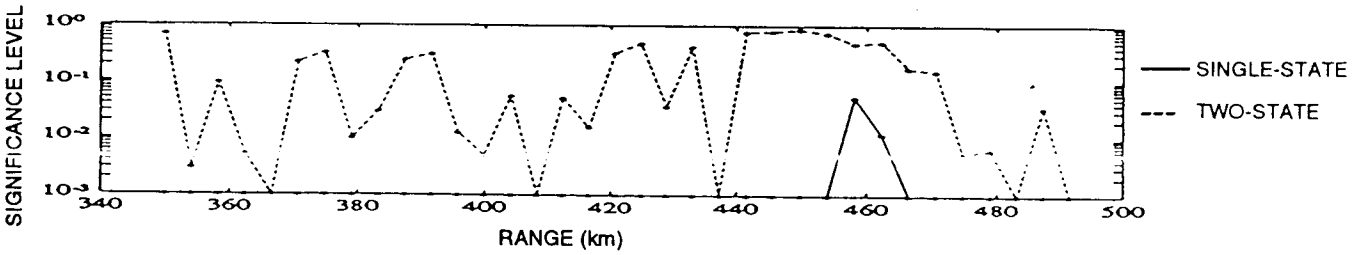

(b) Nature of model

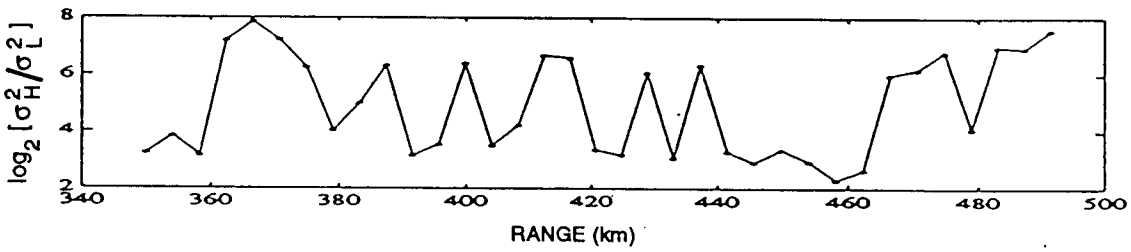

(c) Variance ratio estimates for two-state model

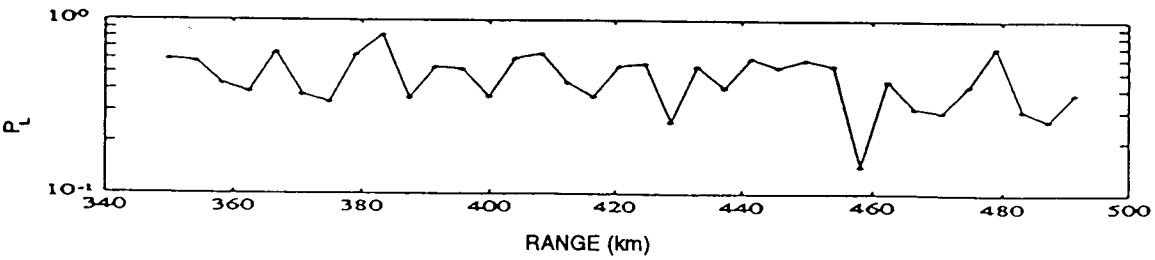

(d) Low-state probability estimates for two-state model

Figure 9. Interferer statistics as a function of range from a moving source and receiving vertical array spatial cell at a depth of 100 meters and a range of 470 kilometers.

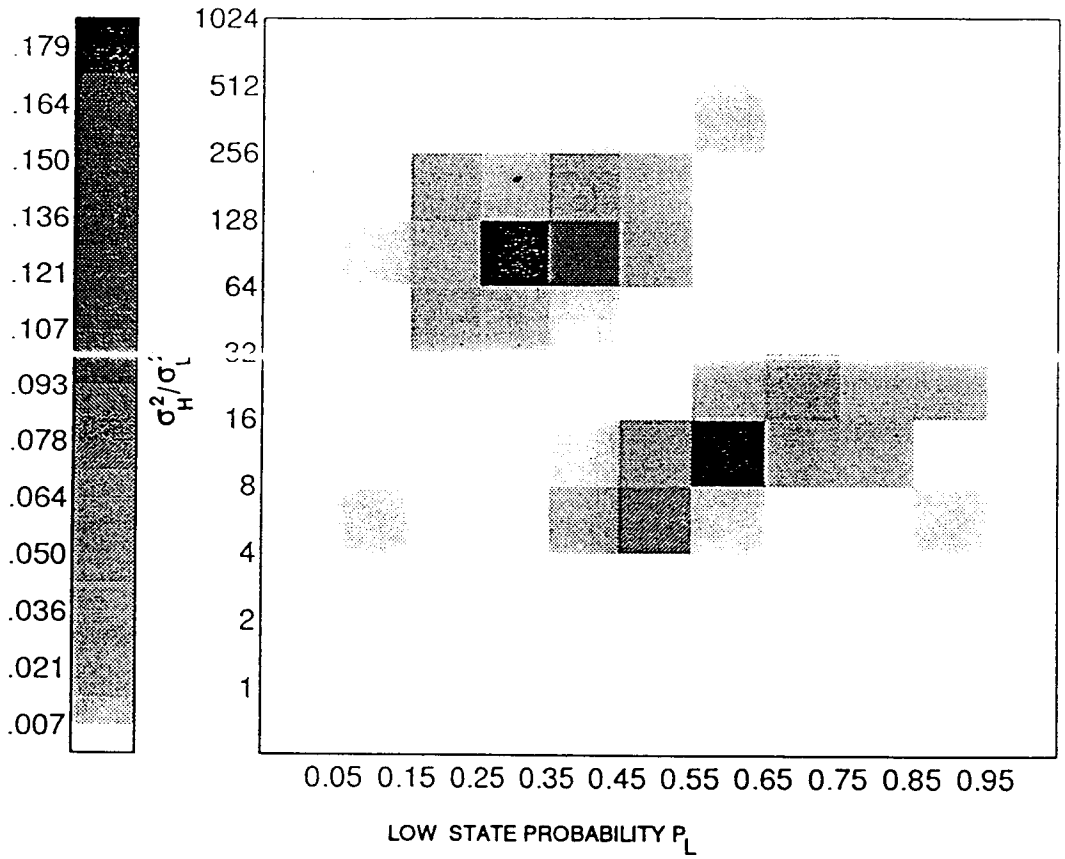

Figure 10. Joint probability density function of low-state probability and state variance ratio for simulated Barlett beamformer cells at a depth of 100 meters and a range of 434, 450, 464, and 470 kilometers.

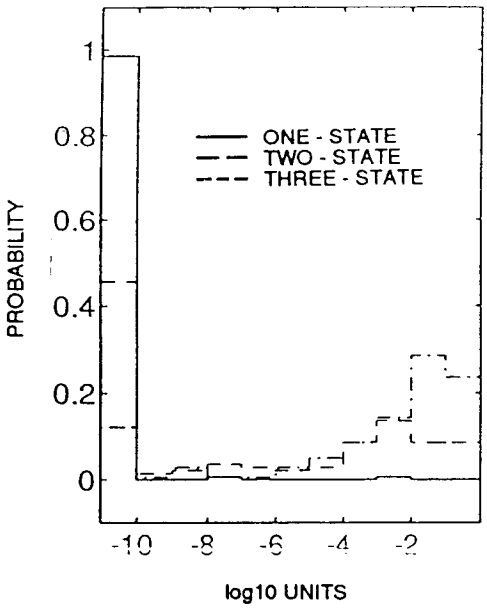

Figure 11. Mixture model Chi-squared test significance levels for beamformed data.

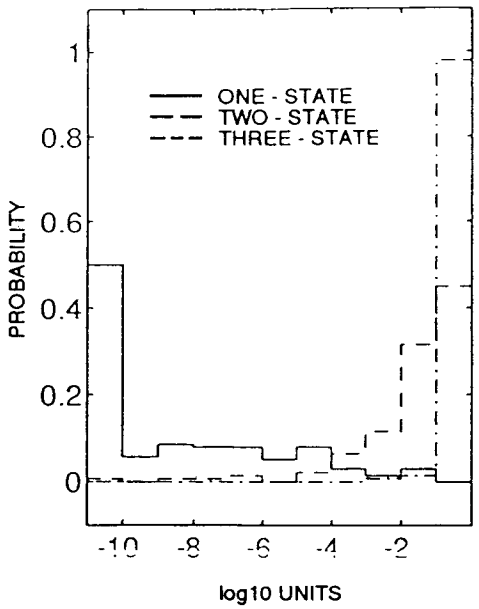

Figure 12. Mixture model Kolmogorov-Smirnov one-sample test significance levels for beamformed data.

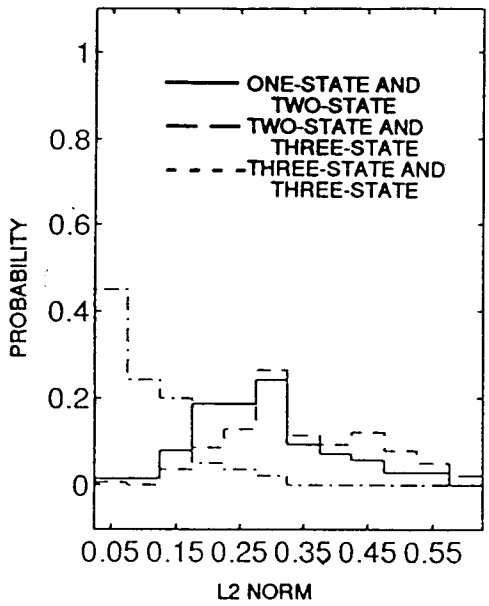

Figure 13. Differences between mixture model probability densities for beamformed data.

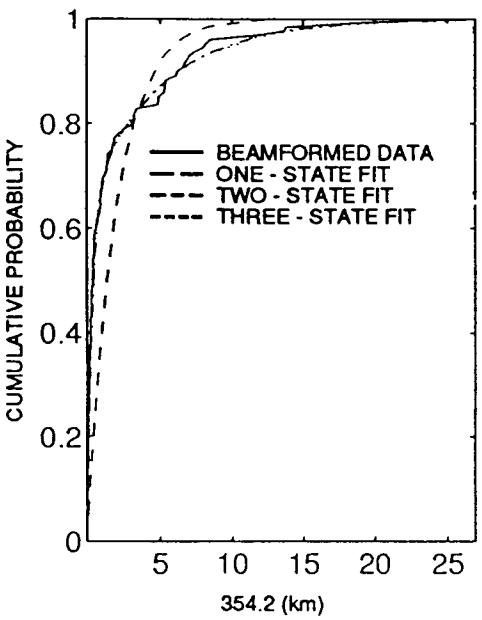

Figure 14. Example of two-state and three-state fits to beamformed data giving nearly equal results.

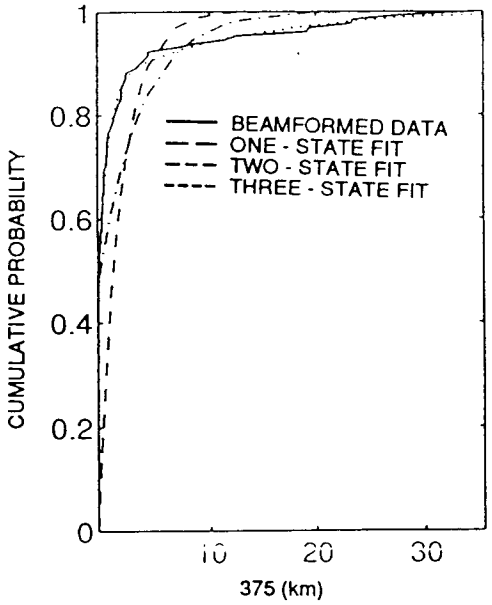

Figure 15. Example of a better three-state than a two-state fit for beamformed data.

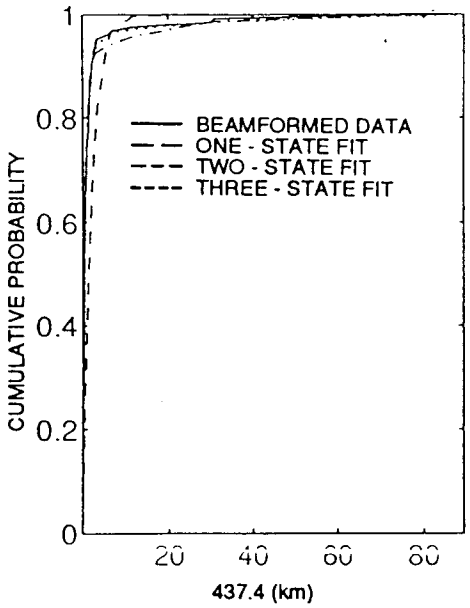

Figure 16. Example of a worse one-state fit to the beamformed data.

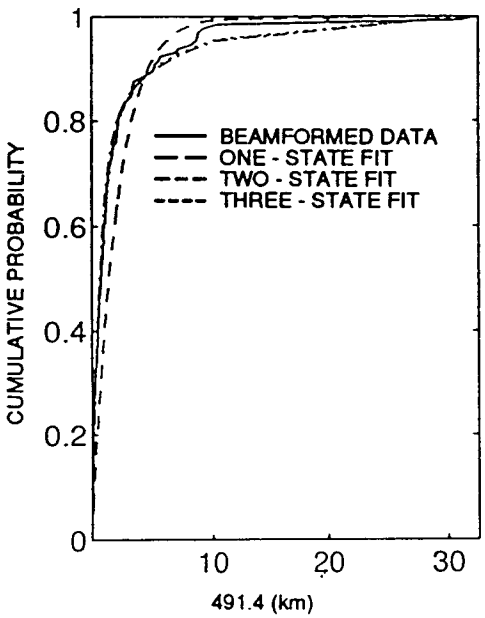

Figure 17. Example of a worse two-state fit to the beamformed data.

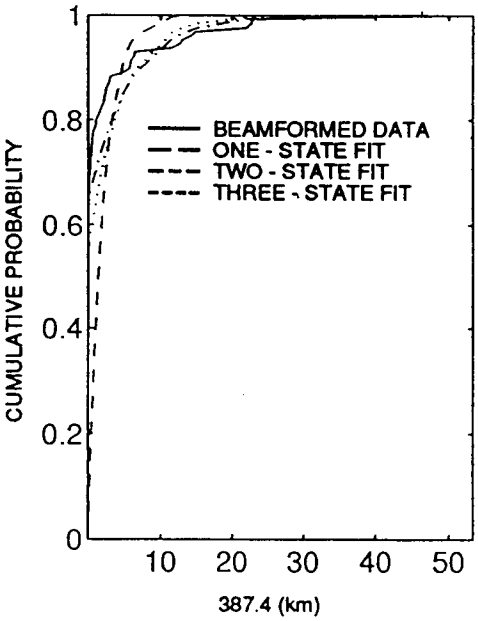

Figure 18. Example of a worse three-state fit to the beamformed data.

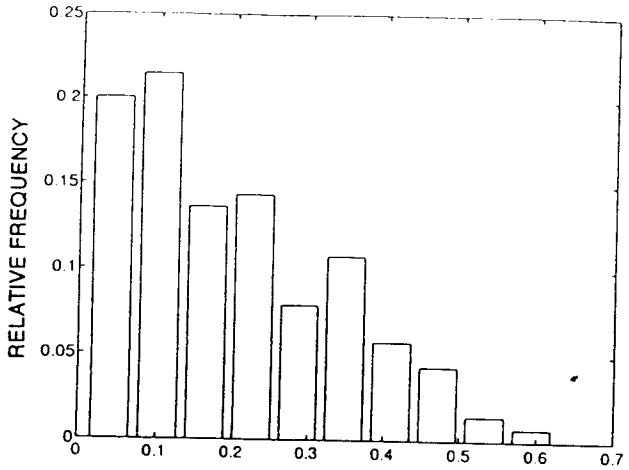

(a) Low-state probability

Figure 19. Three-state parameter distributions for beamformed data.

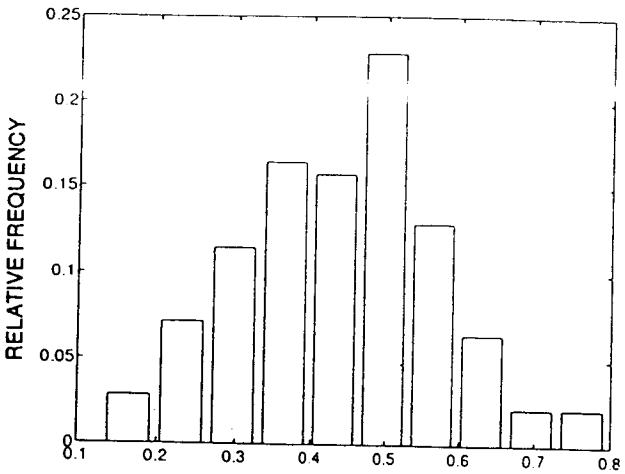

(b) Middle-state probability

Figure 19. (Con't.) Three-state parameter distributions for beamformed data.

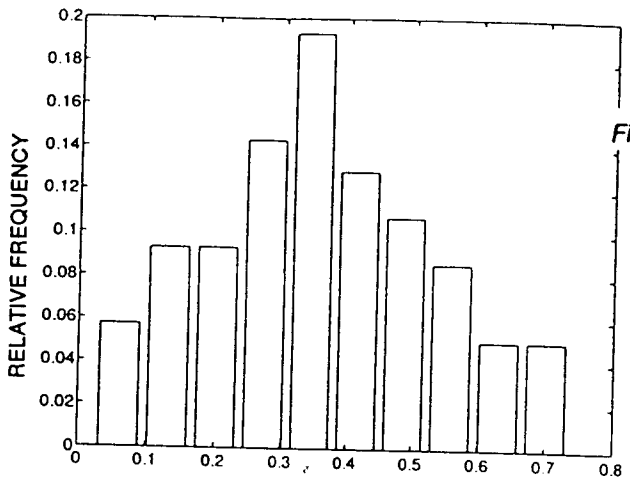

(c) High-state probability

Figure 19. (Con't.) Three-state parameter distributions for beamformed data.

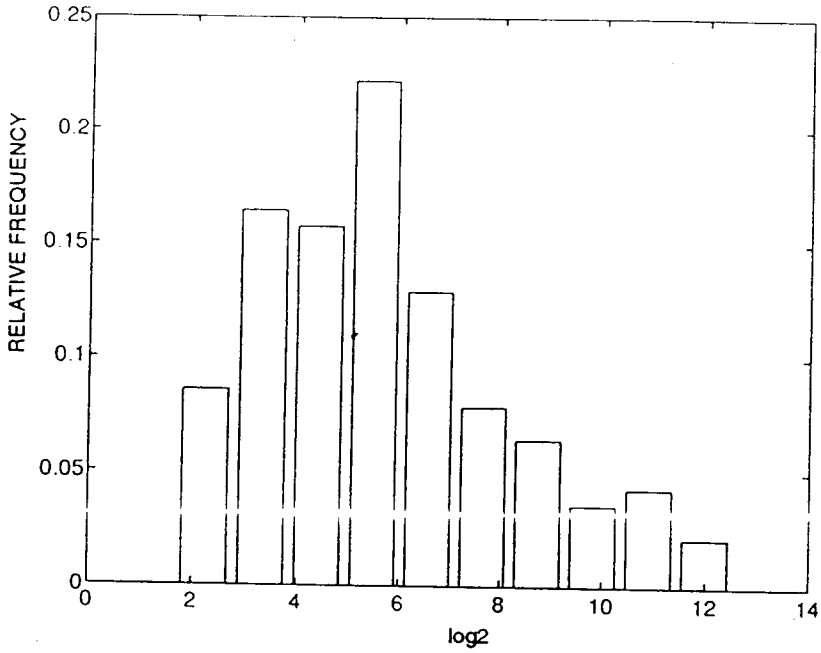

(d) Middle-state to low-state variance

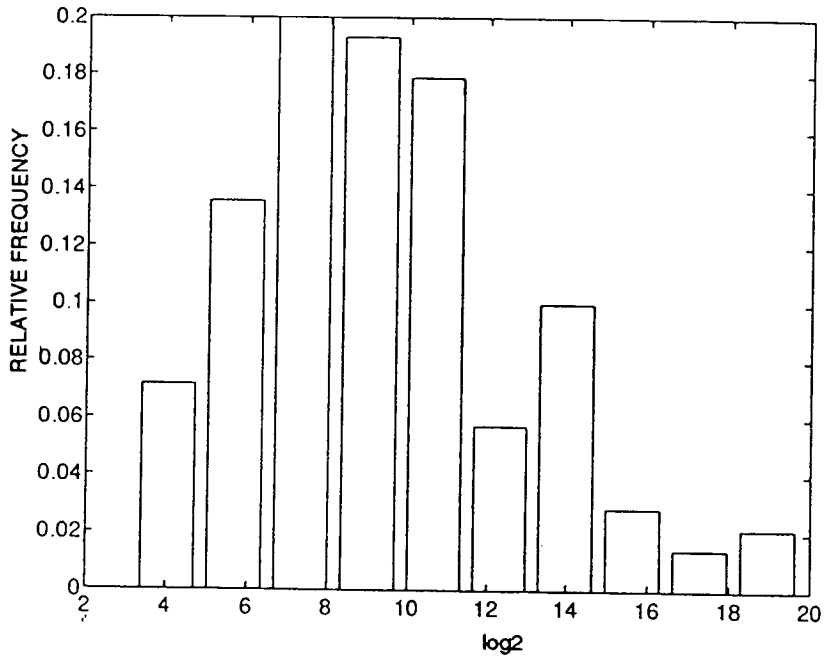

(e) High-state to low-state variance

Figure 19. (Con't.) Three-state parameter distribution for beamformed data.

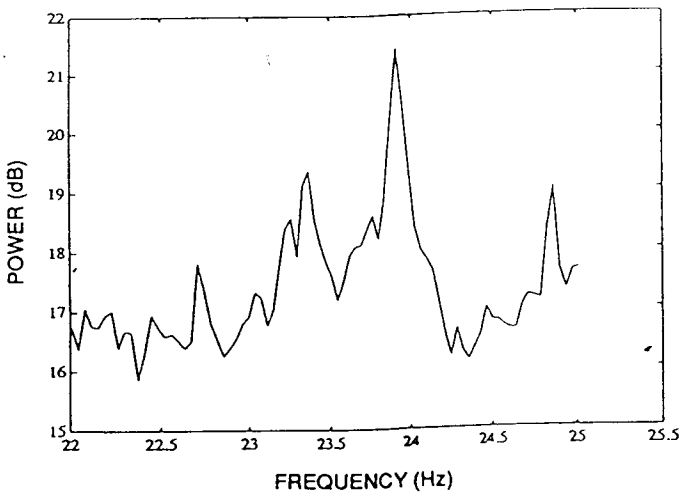

Figure 20. Average power for segment A.

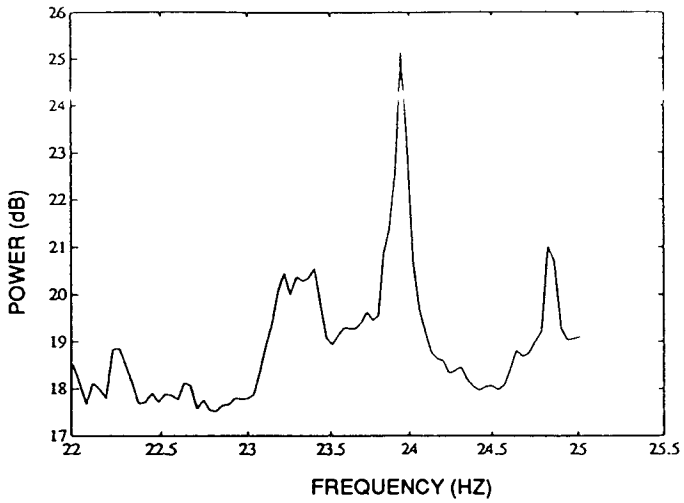

Figure 21. Average power for segment B.

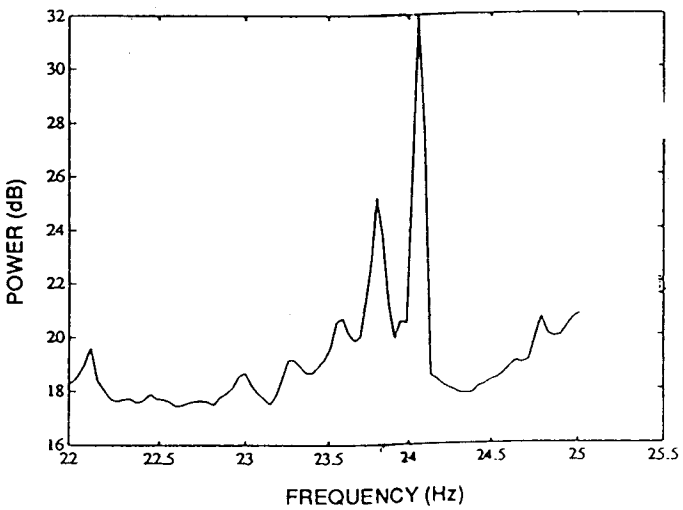

Figure 22. Average power for segment C.

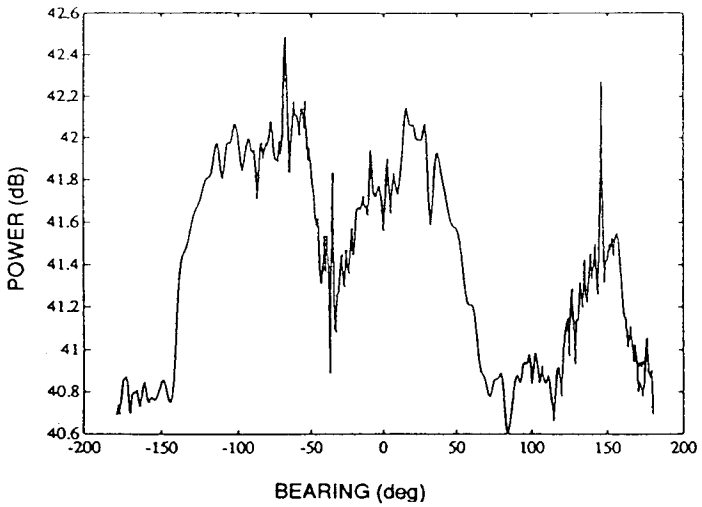

Figure 23. Total 23.914-Hz mode power for segment A.

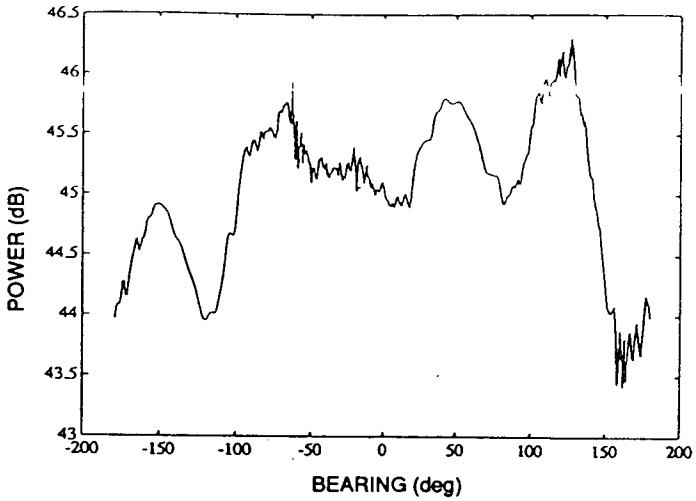

Figure 24. Total 23.950-Hz mode power for segment B.

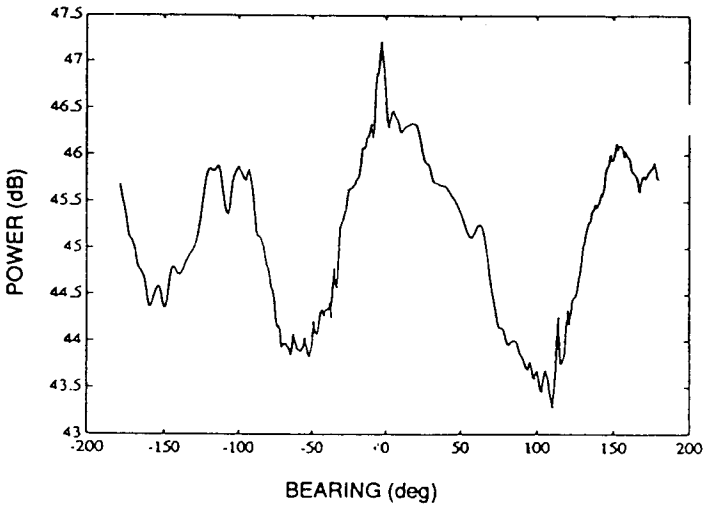

Figure 25. Total 23.804-Hz mode power for segment C.

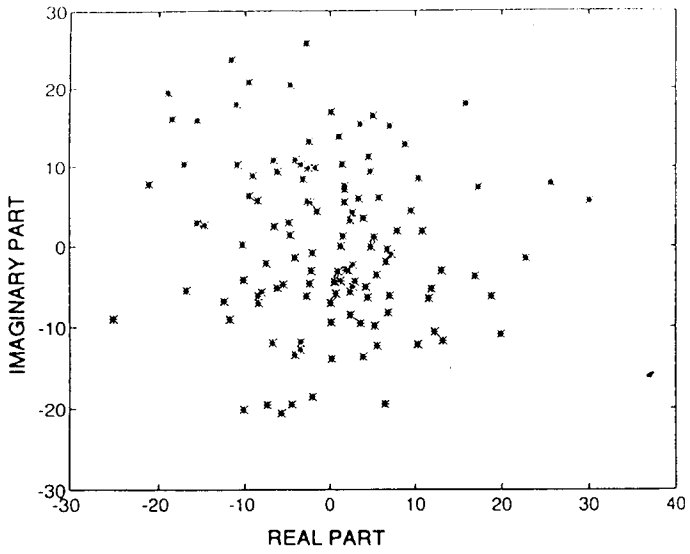

Figure 26. Scatter plot of Fourier coefficients for 23.914-Hz for segment A.

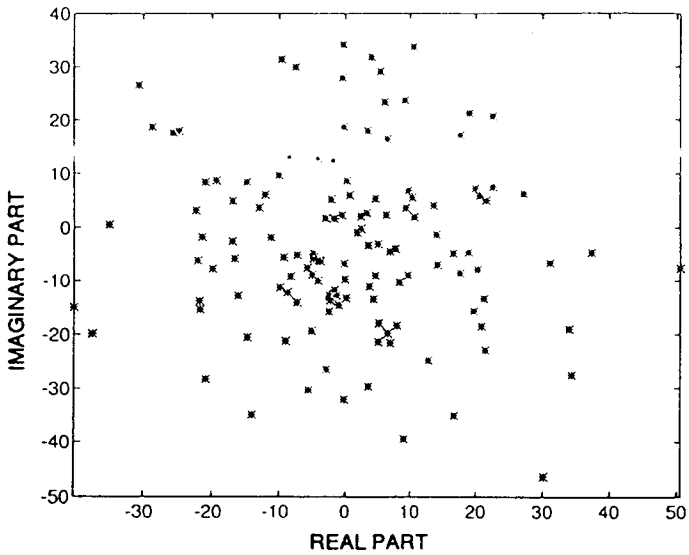

Figure 27. Scatter plot of Fourier coefficients for 23.950-Hz for segment B.

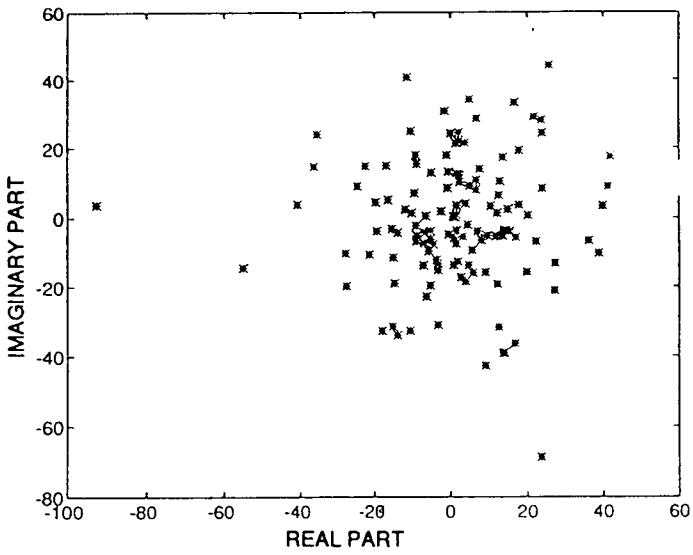

Figure 28. Scatter plot of Fourier coefficients for 23.804-Hz for segment C.

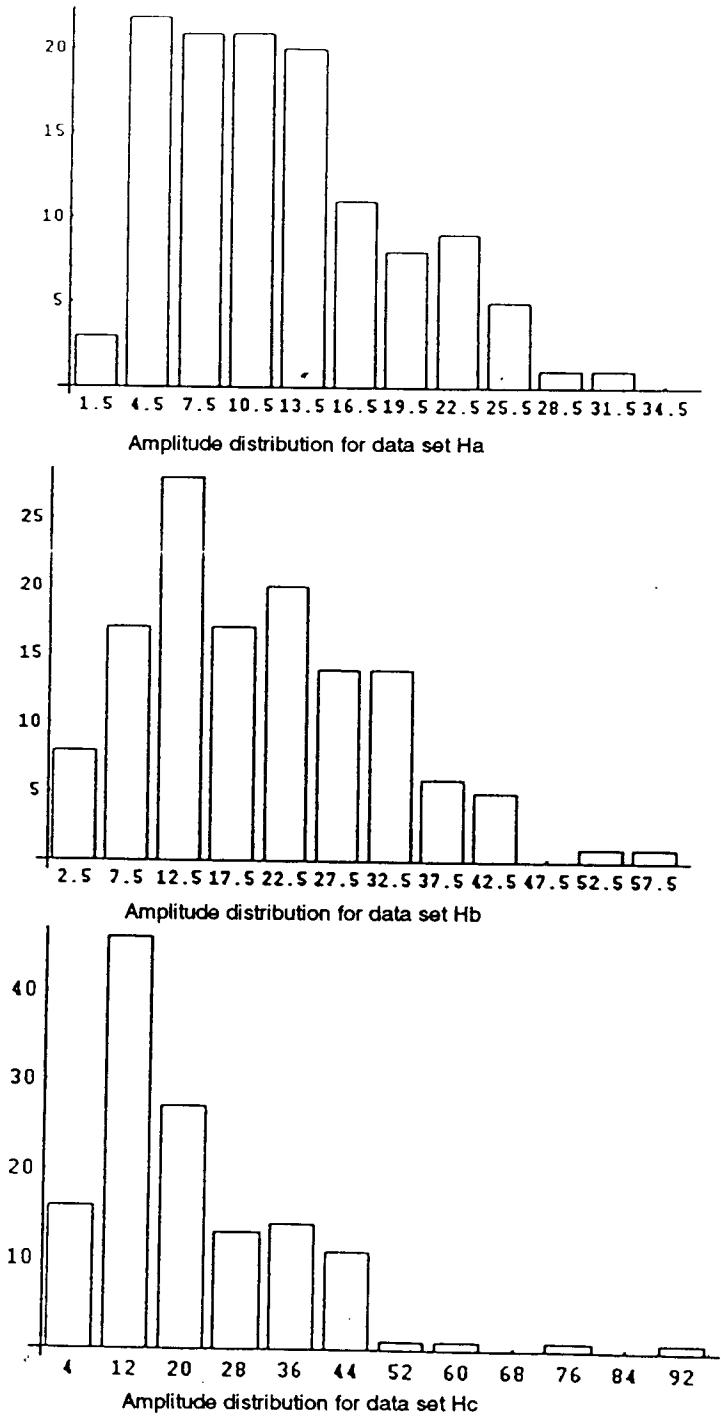

Figure 29. Amplitude distribution of fourier coefficients for selected frequencies for segments A, B, and C.

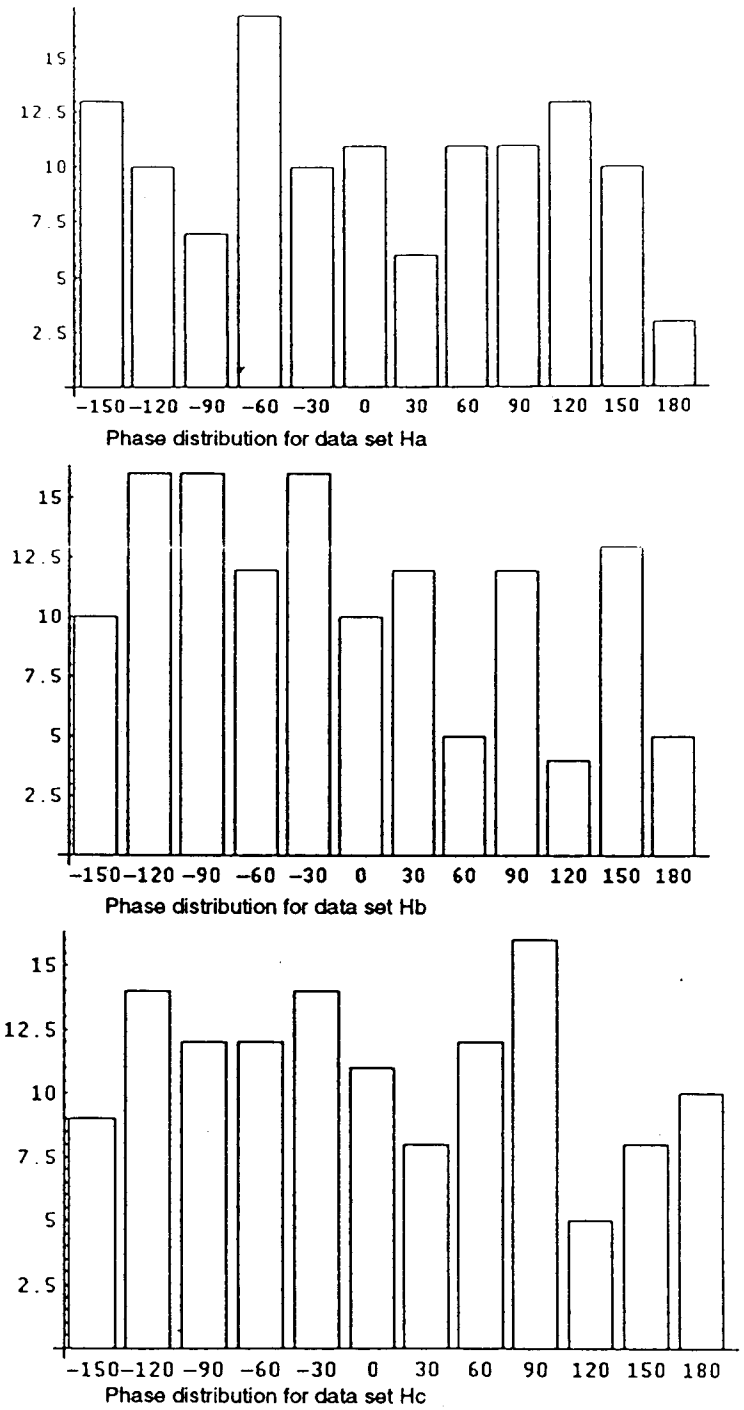

Figure 30. Phase distribution of fourier coefficients for selected frequencies for segments A, B, and C.

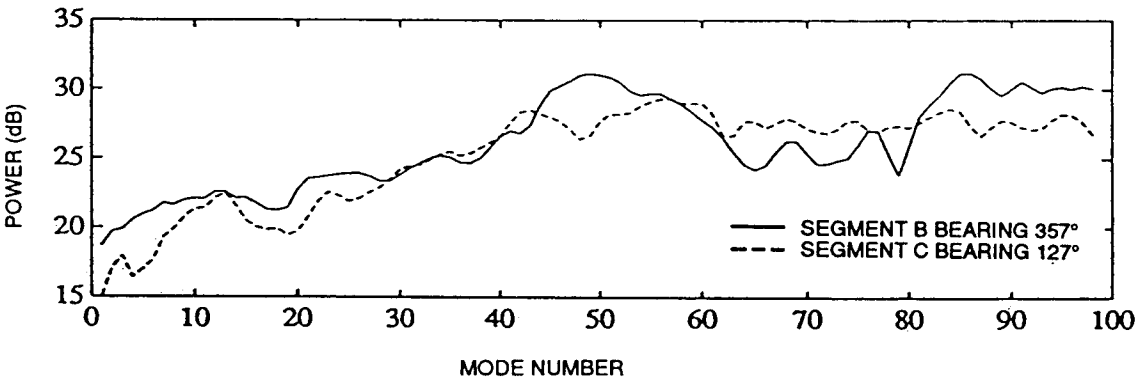

Figure 31. Modal spectra of segments B and C.

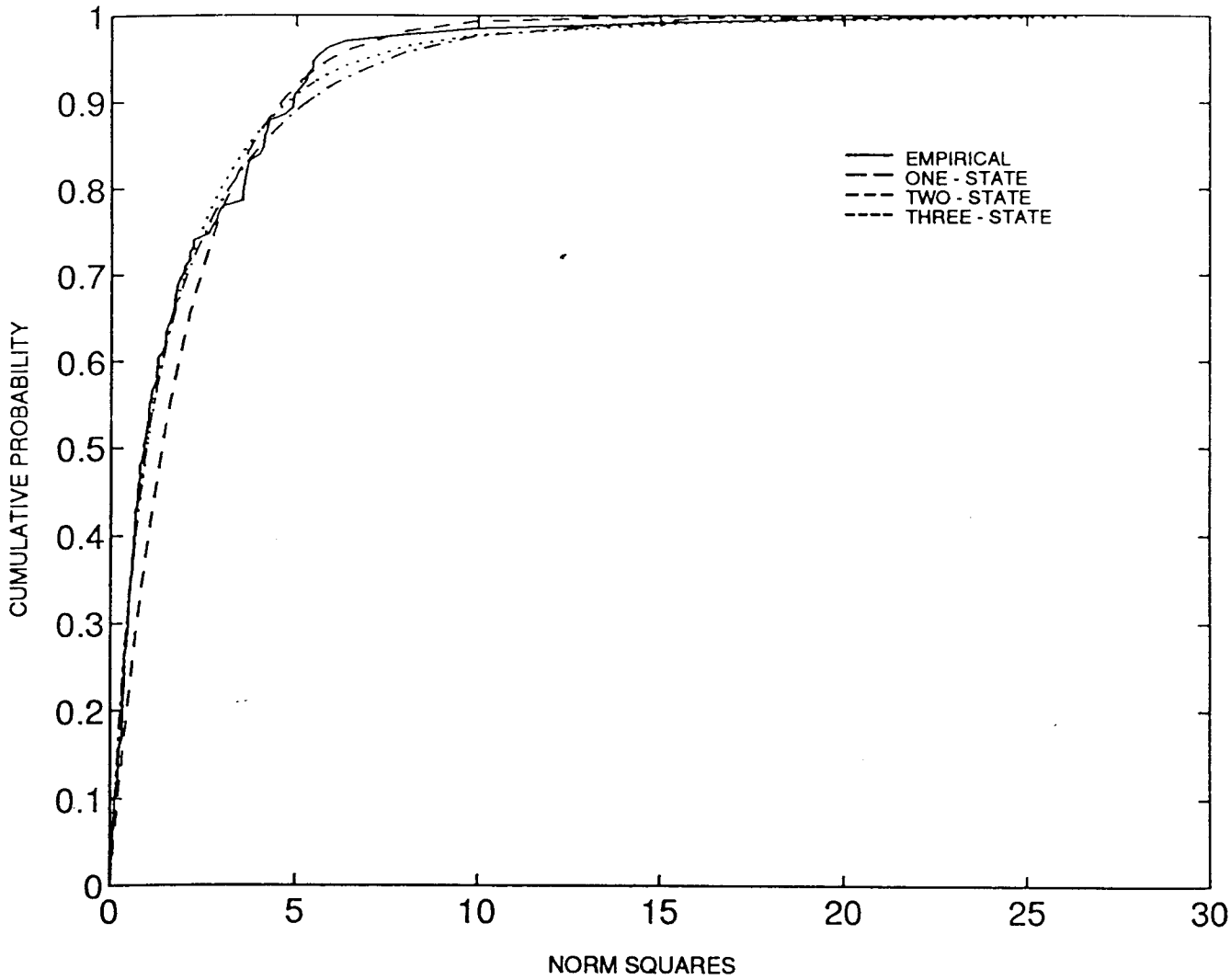

Figure 32. Cumulative probability functions comparison for segment C data.

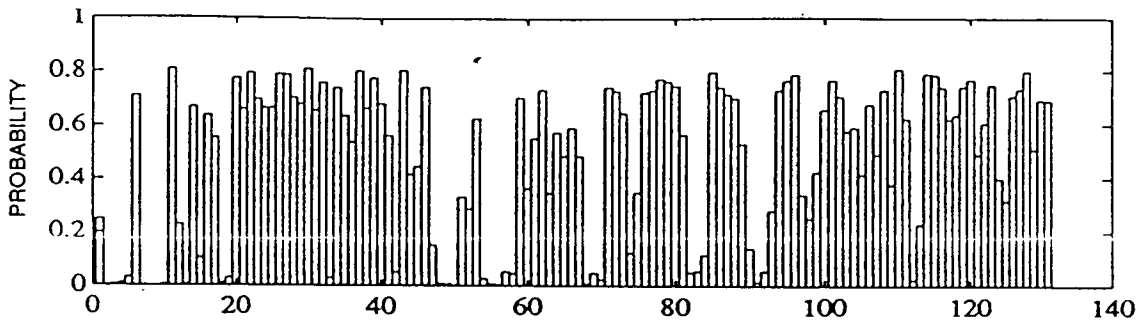

(a) Low-state probability estimates

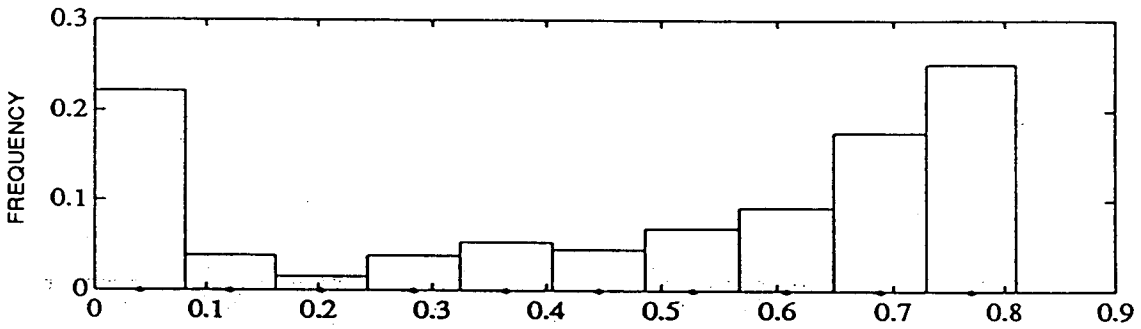

(b) Low-state probabilities

Figure 33. Low-state probability properties for two-state model.

References

Baker, C. R. 1976. "Statistical Tests for the Analysis of Sonar Data", U. S. Navy Underwater Acoustics 26 (2), pp. 227-245.

Baker, C. R. and Gualtierotti, A. F. 1986. "Likelihood Ratios and Signal Detection for Non-Gaussian Processes", in Stochastic Process In Underwater Acoustics, C. R. Baker, Ed. Springer, Verlag, NY.

Baker, C. R. and Gualtierotti, A.F. 1988. "Absolute Continuity and Mutual Information for Gaussian Mixtures", LISS-28, Department of Statistics, University of North Carolina, Chapel Hill, NC.

Baker, C. R. and Gualtierotti, A.F. "Likelihood Ratio Detection of Stochastic Signals," to appear in Advances in Statistical Signal Processing, Volume 2: Signal Detection, H.V. Poor and J. B. Thomas, eds, JAI Press, London, UK.

Berry, L. A. 1981. "Understanding Middleton's Canonical Formula for Class A Noise", IEEE Trans. EMC. 23 (4), pp. 337-344.

Bouvet, M. and Schwartz, S. C. 1988. "Underwater Noises: Statistical Modeling, Detection, and Normalization," J. Acoust. Soc. Am. 83 (3), pp. 1023-1031.

Bouvet, M. and Schwartz, S. C. 1989. "Comparison of Adaptive and Robust Receivers", IEEE Transactions ASSP 37 (5).

Bradley, J. V. 1968. *Distribution Free Statistical Tests*, Prentice Hall, Englewood Cliffs, N.J.

Darling, D. A. 1955. "The Cramer-Smirnov Test in the Parametric Case", Ann. Math. Stat., 26, pp.1-20.

Dempster, A. P., Laird, N.M., and Rubin, D. B. 1977. "Maximum Likelihood from Incomplete Data via the EM Algorithm", J. Roy Stat. Soc. Ser. 39, pp. 1-38.

Heitmeyer, R. M., Davis, L. J. and Yen, N. February 1985. "Implications of Noise Source Resolution on Detection Performance for Horizontal Directional Systems Operating in Ship-Induced Noise Fields", NRL Report 8863.

Heitmeyer, R. M. April 1989. "A model for the Beam Noise Fluctuations for a Horizontal Array Operating in a Ship-Induced Noise Field," Saclantcen Report SR-152.

Hodgkiss, W. 1991. Personal Communication.

Kendall, M., Gibbons, J. D. 1990. *Rank Correlation Methods*, 5th ed., Edward Arnold, London, UK.

Kendall, M., Stuart, A. 1977. *The Advanced Theory of Statistics*, Vol. 1, 4th ed., Macmillan Publishing Co., New York, N.Y.

Kendall, M. and Gibbons, J. D. 1990. *Rank Correlation Methods*, Edward Arnold, London, UK.

Middleton, D. 1966. "Canonically Optimum Threshold Detection", Trans. Inform Theory 12 (2), pp. 230-243.

Middleton, D. 1967. "A Statistically Theory of Reverberation and Similar First-Order Scattered Fields", Trans. Inform. Theory 13 (3), pp. 372-393.

Middleton, D. 1977. "Statistical Physical Models of Electromagnetic Interference", Trans. on EMC 19 (3), pp. 106-127.

Middleton, D. 1983. "Canonical and Quasi-Canonical Probability Models of Class A Interference", IEEE Transactions on EMC 25 (2), pp. 76-106.

Middleton, D. May 1984. "Multiple-Element Threshold Signal Detection of Underwater Acoustic Signals in Non-Gaussian Interference Environments", NOSC CR 23.

Middleton, D. March 12-14, 1991. "Threshold Detection and Estimation in Correlated Interference", 9th Intl. Zurich Symposium on EMC: "EMC '91", Switzerland.

Middleton, D. and Spaulding, A. May 1983. "Optimum Reception in Non-Gaussian Electromagnetic Interference Environments: II Optimum and Suboptimum Threshold Signal Detection in Class A and B Noise", NTIA Report 83-120.

Middleton, D. and Spaulding, A. May 1986. "A Tutorial Review of Elements of Weak Signal Detection in Non-Gaussian EMI Environments", NTIA Report 86-184.

Mohnkern, G. L. February 1989. "Effects of Errors and Limitations on Interference Suppression: Preliminary Report for High-Gain Initiative", NOSC TD 1478.

Porter, 1992. "Kraken Normal Mode Program", Naval Research Laboratory, NRL-MR-5120-92-6920.

Powell, D. R. and Wilson, G. R. 1989. "Class A Modeling of Ocean Acoustic Noise Sources", pp. 17-28, *Topics in Non-Gaussian Signal Processing*, Wegman, E. J., Schwartz, S. C. and Thomas, J. B., eds. Springer-Verlag, New York, N.Y.

Press, W. H., Flannery, B. P., Teukolsky, S. A., and Vetterling, W. T. 1988. *Numerical Recipes in C*, Cambridge University Press, Cambridge, UK.

Reed, I. S., Mallett, J.D., and Brennan, L. E. 1974. "Rapid Convergence Rate in Adaptive Arrays", IEEE Trans. Aerosp. Electron. Sys. 10, pp. 853-863.

Stephens, M. A. 1974. "EDF Statistics for Goodness of Fit and Some Comparisons", J. Am. Stat. Ass. 69 (347), pp. 730-737.

Stephens, M. A. 1976. "Asymptotic Results For Goodness-of-Fit Statistics with Unknown Parameters", The Annals of Statistics, Vol. 4, No. 2, pp. 357-369.

Sukhatme, S. 1972. "Fredholm Determinant of a Positive Definite Kernel of a Special Type and Its Application", The Annals of Mathematical Statistics, Vol. 43, No. 6, pp. 1914-1926.

Tilterington, D.M., Smith, A.F.M., Mackov, U.D. 1985, (reprint 1992). *Statistical Analysis of Finite Mixture Distributions*, Wiley, New York, N.Y.,

Vastola, K. S. 1984. "Threshold Detection in Narrow Band Non-Gaussian Noise, IEEE Transactions Comm. 32 (2), pp. 134-139.

Wilks, S. S. 1962. *Mathematical Statistics*, John Wiley and Sons, New York, N.Y.

Wu, C. F. J. 1983. "On the Convergence Properties of the EM Algorithm," Ann. Stat., 11 (1), pp. 95-103.

Zabin, S. M. and Poor, H. V. 1989. "Parameter Estimation for Middleton Class A Interference Processes", IEEE Transactions Comm. 37 (10), pp. 1042-1051.

Zabin, S. M. and Poor, H.V. 1990. "Recursive Algorithms for Identification of Impulsive Noise Channels," IEEE Transactions Inform. Theory 36 (3), pp. 559-578.

Zabin, S. M. and Poor, H. V. 1991. "Efficient Estimation of Class A Noise Parameters Via the EM Algorithm", Trans. Inform. Theory 37 (1), pp. 60-72.

APPENDIX A
MIXTURE MODEL ESTIMATION AND COMPARISON

This appendix discusses techniques that we used to estimate the parameters of two-state and three-state mixture models and the statistical techniques we used to compare the estimated distributions obtained with the empirical distributions of the data.

Parameter Estimation Techniques.

Four techniques for estimating the parameters of a mixture model with a fixed finite number of states were considered: (1) the method of moments technique, (2) the minimum distance technique, (3) the maximum likelihood technique, and (4) the expectation and maximize (EM) technique. The EM technique was chosen because it was the only estimation technique of the four that can provide accurate estimates of mixture parameters for either a two-state or three-state mixture model given around 100 samples (Zabin and Poor, 1989,1990,1991; Powell and Wilson, 1989). The references in this appendix are listed at the end of the body of this report.

The EM technique is an indirect way of finding the maxima of the likelihood function (Dempster, Laird, and Rubin, 1977). We describe how it can be used to estimate Gaussian mixture parameters. Given an S state Gaussian mixture model and N data samples $\{z_j | 1 \le j \le N\}$, the main difficulty in estimating the mixture model parameters is that the partitioning of samples z_j by states is unknown. Let α denote the S mixture model parameter set $\{p_1, \sigma_1^2, p_2, \sigma_2^2, ..., p_S, \sigma_S^2\}$, which is to be estimated from the data samples.

A description of the EM technique involves two likelihood functions, an incomplete log likelihood function $L(\{z_j\}|\alpha)$ and a complete log likelihood function $CL(\{(z_j, s_j)\}|\alpha)$ defined as follows:

$$L(\{z_j\}|\alpha) = \sum_{j=1}^{N} \ln p(z_j|\alpha)$$

and

$$CL(\{(z_j, s_j)\}|\alpha) = \sum_{j=1}^{N} \ln p((z_j, s_j)|\alpha) \ ,$$

where $p(z_j|\alpha)$ is the probability of z_j occuring given α and $p((z_j, s_j)|\alpha)$ is the probability of z_j occuring in state s_j, the state containing it, given α.

The EM technique constructs a family of estimates of the vector α:

$$\alpha_1, \alpha_2, ..., \alpha_n, ..., \text{ where } \alpha_n = (p_{n,1}, \sigma_{n,1}^2, p_{n,2}, \sigma_{n,2}^2, ..., p_{n,S}, \sigma_{n,S}^2).$$

One estimate is obtained for each initial set of parameters and then the best estimate of the parameters after iteration of the EM process is chosen as the estimate of the parameters. In particular, given the parameter vector estimate α_n the parameter estimate α_{n+1} is constructed as follows:

Step 1. Select a set of initial parameter vectors that span reasonable models for the data being fitted. (This step becomes increasingly difficult as the number of parameter values increases and places a practical limit on the number of states in the mixture model for which the technique can be used to estimate state parameters.) Choose a vector α_1 from the set of initial parameter vectors to be recursively refined to a candidate estimate of α

Step 2. Given the estimate $\alpha_n, n = 1, 2, \ldots$, calculate the conditional probabilities of the states given z_j and α_n:

$$p(s_j = k|z_j, \alpha_n) = \frac{p(z_j|s_j = k, \alpha_n)p_{n,k}}{\Sigma_{h=1}^{S} p(z_j|s_j = h, \alpha_n)p_{n,h}},$$

where

$$p(z_j|s_j = h, \alpha_n) = \frac{1}{2\pi\sigma_{n,h}^2} e^{-\frac{|z_j|^2}{2\sigma_{n,h}}} \text{ for } 1 \le h \le S.$$

Step 3. Construct α_{n+1} by setting

$$p_{n+1,k} = \frac{1}{N}\sum_{j=1}^{N} p(s_j = k|z_j, \alpha_n) \text{ for } 1 \le k \le S$$

and

$$\sigma_{n+1,k} = \frac{1}{N}\sum_{j=1}^{N} \frac{|z_j|^2}{2p_{n+1,k}} p(s_j = k|z_j, \alpha_n) \text{ for } 1 \le k \le S.$$

Step 4. Discontinue the estimation process after the successive estimates cease to change significantly, draw a new parameter vector from the set of initial parameter vectors, and start a new estimation process to refine it.

Step 5. Calculate $L(\{z_j\}|\alpha)$ for each of the final estimates obtained by refining the different initial parameter vectors. Take as the best estimate of the parameter vector the final estimate which maximizes $L(\{z_j\}|\alpha)$.

For a Gaussian mixture model α_{n+1} is a maximum or saddle point of the expected value of the complete likelihood function

$$ECL(\alpha_{n+1}) = \sum_{j=1}^{N}\sum_{k=1}^{S} \ln(p((z_j, s_j = k)|\alpha_{n+1}))p(s_j = k|z_j, \alpha_n).$$

Wu (1983) has shown under conditions that hold for estimating Gaussian mixture models, that a sequence of estimates of the expected value of the complete likelihood function converges to a saddle point or local maximum of the incomplete likelihood function $L(\alpha)$. When this is the case, a good approximation of the best parameter vector can be obtained by selecting the vector that maximizes the incomplete likelihood function from the parameter vectors obtained using the EM algorithm for a well-chosen set of initial parameter vectors.

The above technique can easily be applied to the estimation of the best two-state Gaussian mixture model. For this case, the number of parameters can be reduced in the following way. The Fourier coefficients $\{z_j\}$ are normalized so that the normalized coefficients have a mean norm squared value of 2. In addition, the search need only be made over p_L, the low-state probability, and over σ_L^2, the low-state variance, since the high-state probability $p_H = 1 - p_L$ and the high-state variance $\sigma_H^2 = \frac{1 - p_L\sigma_L^2}{p_H}$. Furthermore, both the low-state probability and low-state variance are constrained to values between 0 and 1 for the normalized data. The EM algorithm can be used to search for the best two-state model by initiating searches for each pair of parameter values (p_L, σ_L) in $\{(.1, .1), (.1, .5), (.1, .9), (.5, .1), (.5, .5), (.5, .9), (.9, .1), (.9, .5), (.9, .9)\}$. This was the approach taken to fit data by a two-state Gaussian mixture model whenever the EM algorithm was used.

Computer simulations were used to characterize the performance of the EM algorithm as described to determine two-state Gaussian mixture model parameters as a function of N, p_L and $\rho = \frac{\sigma_H^2}{\sigma_L^2}$. For each p_L in {0.01, 0.05, 0.1, 0.2, 0.4, 0.8, 0.9, 0.95, 0.99}, ρ in { 1.6, 6.25, 25, 100},and N in {16, 31, 62, 125, 250, 500, 1000}, 100 sets of data were generated and the mean squared errors in the estimated parameters p_L and σ_L^2 were calculated.

Figures A-1a and 1b present mean square error estimates of p_L and σ_L^2 as a function of sample size N for a Gaussian mixture models with two fairly distinct states, $p_L = 0.4$ and $\rho = 6.25$. These curves indicate that even for N = 16, the EM procedure could estimate the state parameters with less than 8% error. Figures A-2a and 2b present mean square estimates for p_L and σ_L^2 as a function of p_L for $\rho = 6.25$ and $N = 125$, while figures A-3a and 3b present them as a function of ρ for $p_L = 0.4$ and $N = 125$. Observe that the estimation process leads to reasonable estimates (10% or less mean square error in the parameter estimated) for 125 samples provided the low-state probability is greater than about 0.20. Figure A-4, based on data compiled from all of the simulations discussed here, indicated that 90% of the time fewer than 50 iterations were required for convergence.

The best two-state Gaussian mixture model parameters can be used to initiate a search for the best three-state Gaussian mixture model. The two-state process results in the parameter set $\{p_{2,L}, \sigma_{2,L}^2, p_{2,H}, \sigma_{2,H}^2\}$ for normalized data with variance 1. Any three-state fit would lead to a new middle state with probability $p_{3,M}$ and variance $\sigma_{3,M}^2$ with $\sigma_{2,L}^2 \le \sigma_{3,M}^2 \le \sigma_{2,H}^2$ and low-state and high-state parameter set $\{p_{3,L}, \sigma_{3,L}^2, p_{3,H}, \sigma_{3,H}^2\}$ with $0 \le p_{3,L} \le p_{2,L}$, $\sigma_m^2 \le \sigma_{3,L}^2 \le \sigma_{2,L}^2$, where σ_m^2 is the minimum norm square of any of the samples, and $\sigma_{3,L}^2 \le \sigma_{3,M}^2 \le \sigma_{3,H}^2$. The number of initial parameter vectors was further reduced by choosing state probabilities and variances in a manner consistent with the data.

Given $\sigma_{3,M}^2$ with $\sigma_{2,L}^2 \le \sigma_{3,M}^2 \le \sigma_{2,H}^2$ and $p_{3,M}$ with $0 \le p_{3,M} \le 1$ partition the samples into sets S_L, S_M, and S_H. Let S denote the set of samples from which the model is to be estimated. Order the norms of the elements of S from low to high and let S_M consist of the $100p_{3,M}$ of the elements of S with norm squares closest to $\sigma_{3,M}^2$. Let S_L consist of the elements of S with norm squares less than or equal to the norm squares of the elements of S_M and let S_H consist of the remaining elements of S. Then let $p_{3,L}$ be the number of elements in S_L divided by the number of elements in S and let $\sigma_{3,L}^2$ be the average value of the norm squares of the elements in S_L; let $p_{3,H}$ be the number of elements in S_H divided by the number of elements in S and let $\sigma_{3,H}^2$ be the average value of the norm squares of the elements in S_H. We choose three values of the middle state variance and three values of the middle state probabilities to obtain 8 initial parameter estimates to estimate three-state parameter vectors using the EM algorithm given a two-state model of the data. The three variances were $\sigma_{3,M}^2 = .8\,\sigma_{2,L}^2 + .2\sigma_{2,H}^2$, $\sigma_{3,M}^2 = .5\,\sigma_{2,L}^2 + .5\sigma_{2,H}^2$, and $\sigma_{3,M}^2 = .2\,\sigma_{2,L}^2 + .8\sigma_{2,H}^2$; the three low-state probabilities were 0.2, 0.5, and 0.8. This initialization procedure was used to estimate three-state Gaussian mixture model parameters whenever the EM algorithm was used to obtain such estimates.

Simulations were conducted to determine the ability of the EM algorithm to distinguish between a circular Gaussian distribution and a two-state Gaussian mixture model. This was accomplished by determining the distribution of the two-state mixture parameters when the input data were drawn from a circular Gaussian distribution. For Gaussian noise, either the probabilities of one of the states should be near zero, or the ratio of the variances should be near 1. Figure A-5a shows the parameters estimated for 1280 sets of 130 samples drawn from a zero-mean unit variance circular Gaussian distribution. Figures A-5b, c, and d are the cumulative

distributions of the ratio of the estimated variances for those points in figure A-5a satisfying $0.1 \le p_L \le 0.9$, $0.2 \le p_L \le 0.8$, and $0.3 \le p_L \le 0.7$, respectively. These plots can be used to estimate certain joint probabilities such as $P(\frac{\sigma_H^2}{\sigma_L^2} \ge 4 \text{ and } 0.2 \le p_L \le 0.8) = (0.05)(0.136) = 0.0068$ for Gaussian input.

Monte Carlo studies were also done to determine the distribution of the two-state mixture model parameters when the input data were obtained from a sinusoid in white Gaussian noise. The Fourier transform of such data in the frequency bin containing the signal is the sum of noise data, which has a zero-mean circular Gaussian density and a complex sinusoid. For different choices of the amplitude and precession rate of the complex sinusoid, 1280 independent sets of 130 samples were generated, and the EM algorithm was run on these data. Figures A-6a, b, and c show the distribution of the estimated variance ratio $\frac{\sigma_H^2}{\sigma_L^2}$ and low-state probability p_L for signal-to-noise ratios of 1.8, 4.8, and 7.8 dB, respectively, and a precession rate of 0.5π rad/(FFT sample). This precession rate corresponds to the signal frequency lying midway between two center frequencies of the FFT and using a window with 50% overlap in the calculation of the FFT. The precession rate had very little impact on the distribution of the estimated parameters in this study.

Figure A-5 suggests that for a set of 130 samples having a Gaussian distribution, the EM algorithm is unlikely to estimate the Gaussian mixture parameters p_L and $\frac{\sigma_H^2}{\sigma_L^2}$ satisfying $0.2 \le p_L \le 0.8$ and $\frac{\sigma_H^2}{\sigma_L^2} > 4$. Figure A-6 suggests that the EM algorithm is unlikely to estimate a significant amount of mixing in successive Fourier coefficients of a sinusoid in Gaussian noise. Furthermore, as the signal-to-noise ratio increases the estimated parameters of the successive Fourier coefficients of the signal-plus-noise process stabilize at values that indicate essentially no mixing.

Statistical Tests to Compare Interference Models.

Statistical tests were selected to characterize the various features of the complex samples of interference data. In particular, statistical tests were selected to determine the suitability of modeling the interference data statistics by a spherical Gaussian distribution or as a Gaussian mixture distribution. These tests were used to analyze simulated data and MDA hydrophone data. This section briefly describes the statistical techniques that are used in our discussion of information processing.

Both spherical Gaussian and Gaussian mixture models require that the real and imaginary baseband sample components are zero-mean and identically distributed. The two models are distinguished by the fact that for a Gaussian model the statistics are stationary and for a Gaussian mixture model nonstationary. Therefore, statistical tests were selected to evaluate the hypotheses that the real and imaginary baseband sample components of narrowband interference are stationary, independent, and have Gaussian distributions, and that the real and imaginary parts are independent of each other. If these conditions hold and the variance of the real part is equal to the variance of the imaginary part, the probability distribution of the complex interference samples is a spherical Gaussian distribution. In addition, statistical tests were selected to determine whether the interference data were best described by either a one-state, two-state, or three-state Gaussian mixture model.

The Kendall-Mann tau test (Baker, 1976; Bradley, 1968; Kendall and Gibbons, 1990) was used to determine the presence of trends in the mean and variance of the interference data. This test is an application of the Kendall rank correlation test. It is used to evaluate the independence of two time series of real numbers by searching for a relationship in the ordering by magnitude of the two time series. Each time series is assumed to consist of independent, identically distributed data. (The present description assumes that each time series is without ties, i.e. $x_i \ne x_j$ and $y_i \ne y_j$ for $i \ne j$. See Kendall and Gibbons (1990) for the modifications necessary to cover the

case of possible ties.) The Kendall rank correlation test evaluates the hypothesis that the two time series $\{x_i | 1 \le i \le N\}$ and $\{y_i | 1 \le i \le N\}$ consist of independent identically distributed data.

The Kendall rank correlation test statistic is formed by ordering the pairs (x_i, y_i) according to the magnitude of the x coordinate from its smallest value to its largest value. Let $\{(x_{i^\wedge}, y_{i^\wedge})\} = \{(x_i, y_i) | 1 \le i \le N\}$ with $x_{i^\wedge} < x_{j^\wedge}$ if $i^\wedge < j^\wedge$. For each $i^\wedge$, let $I_{i^\wedge}$ denote the number of indices $j^\wedge > i^\wedge$ with $y_{j^\wedge} < y_{i^\wedge}$ and $T_{i^\wedge}$ denote the number of indices $j^\wedge > i^\wedge$ with $y_{j^\wedge} > y_{i^\wedge}$. Then the test statistic is $S = \frac{2(T-I)}{N(N-1)}$, where $T = \sum_{i^\wedge=1}^{N} T_{i^\wedge}$ and $I = \sum_{i^\wedge=1}^{N} I_{i^\wedge}$. If the time series $\{x_i | 1 \le i \le N\}$ and $\{y_i | 1 \le i \le N\}$ are independent, then the distribution of S is independent of their distributions and approaches a zero-mean normal distribution with variance $\frac{2(2N+5)}{9N(N-1)}$. The Kendall rank correlation test can be used for sample sizes larger than 30. The Kendall-Mann tau test is applied to a single real-time series $\{y_i | 1 \le i \le N\}$ by setting $x_i = i$ and applying the Kendall rank correlation test. Applied in this manner, the Kendall-Mann tau test detects trends in the mean of the elements of $\{y_i | 1 \le i \le N\}$. Applied to the real-time series $\{|y_i| \, | 1 \le i \le N\}$, it detects trends in the variances of the elements of $\{|y_i| \, | 1 \le i \le N\}$.

The Kolmogorov-Smirnov two-sample test was used as an additional test of the stationarity of the real and imaginary interference data, and it was used to test the equality of the distributions between the real and imaginary components of the complex valued interference samples. If $\{x_i | 1 \le i \le N\}$ and $\{y_i | 1 \le i \le N\}$ are two time series, the two-sample test measures the equality of the distributions of $\{x_i | 1 \le i \le N\}$ and $\{y_i | 1 \le i \le N\}$ based on the maximum of the absolute value of the difference between their cumulative distributions (Baker, 1976; Bradley, 1968). The resulting stationarity test for a real-valued $\{x_i | 1 \le i \le N\}$ is the Kolmogorov-Smirnov two-sample test applied to $\{x_i | 1 \le i \le M\}$ and $\{x_i | M+1 \le i \le N\}$, where M is the greatest integer less than or equal to $\frac{N}{2}$. Assuming that the two distributions are identical, the distribution of the statistic is independent of the distribution of the random variables and is given by an infinite sum, which is commonly approximated by its first few terms (Press et al., 1988; Wilks, 1962).

The Kolmogorov-Smirnov one-sample test was used to compare empirical distributions with fixed distributions, e.g., the Gaussian and the exponential distributions. The statistic is the maximum of the absolute value of the difference between the hypothetical cumulative distribution and the empirical cumulative distribution. The distribution on the statistic is similar to that of the Kolmogorov-Smirnov two-sample test (Press et al, 1988).

The Chi-squared test (Press et al, 1988) was also used to compare empirical density functions and model density functions. This test requires that the data be placed in bins. The statistic is formed by summing (over all bins) the normalized square of the difference between the expected number of data points in each bin, based on the theoretical distribution, and the realized number in each bin. The normalization factor is the expected number of data points per bin. Assuming that the theoretical distribution is correct, as the number of samples goes to infinity, the distribution of the statistic approaches a Chi-squared distribution on B-r-1 degrees of freedom, where B is the number of bins into which the data are divided and r is the number of parameters estimated from the data. The level of significance obtained for the Chi-squared accounts for the number of estimated distribution parameters. The level of significance obtained for the Kolmogorov-Smirnov one-sample test does not account for the number of estimated distribution parameters; correction factors are available for the Kolmogorov-Smirnov one-sample test for special cases (Stephens, 1974).

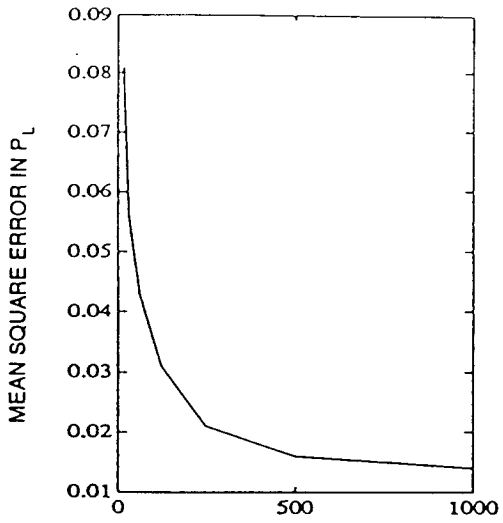

(a) Sample Size

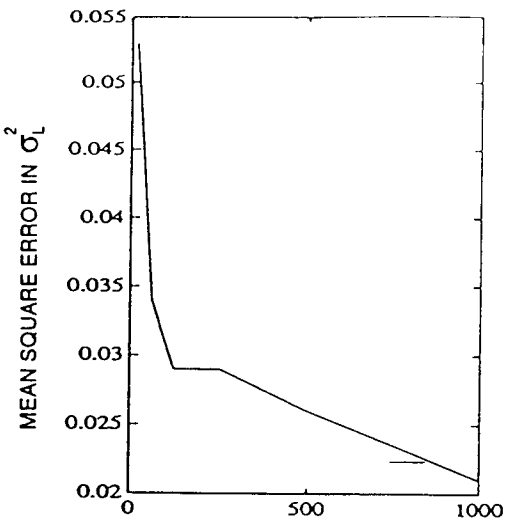

(b) Sample Size

UNCLASSIFIED

Figure A-1. Mixture model parameter errors as a function of sample size.

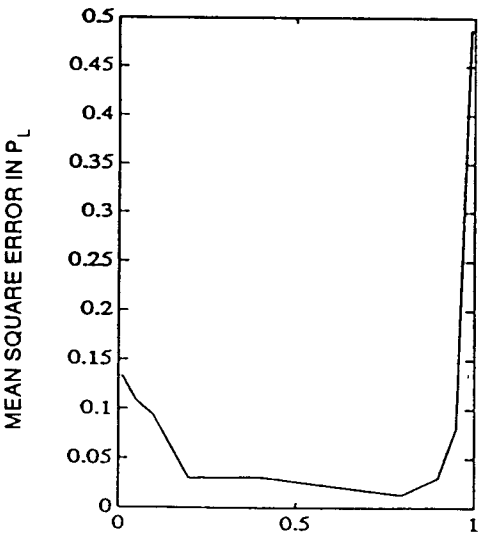

(a) Low-state probability

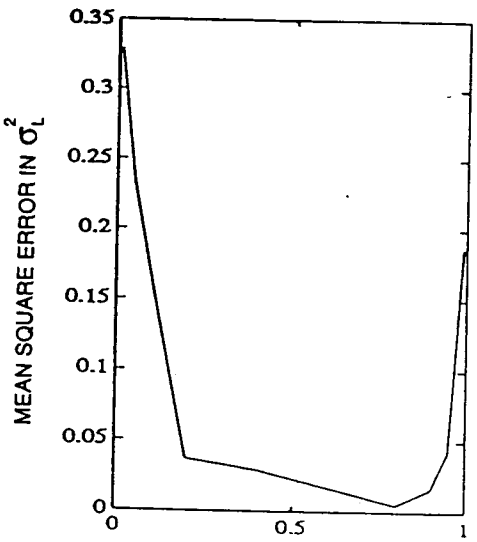

(b) Low-state probability

Figure A-2. Mixture model parameter errors as a function of low-state probability.

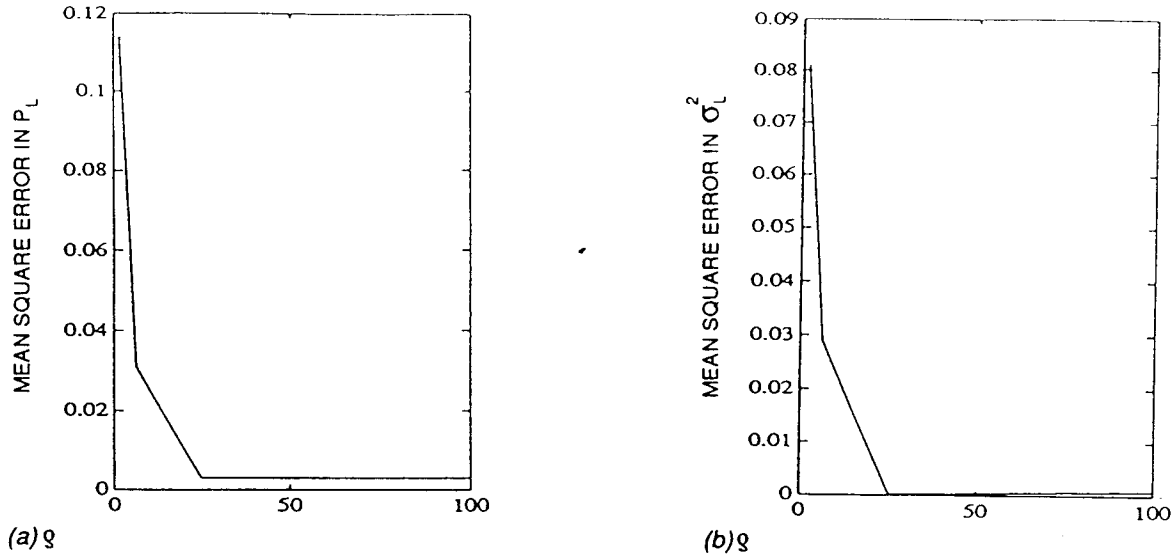

Figure A-3. Mixture model parameter errors as a function of the ratio of variances.

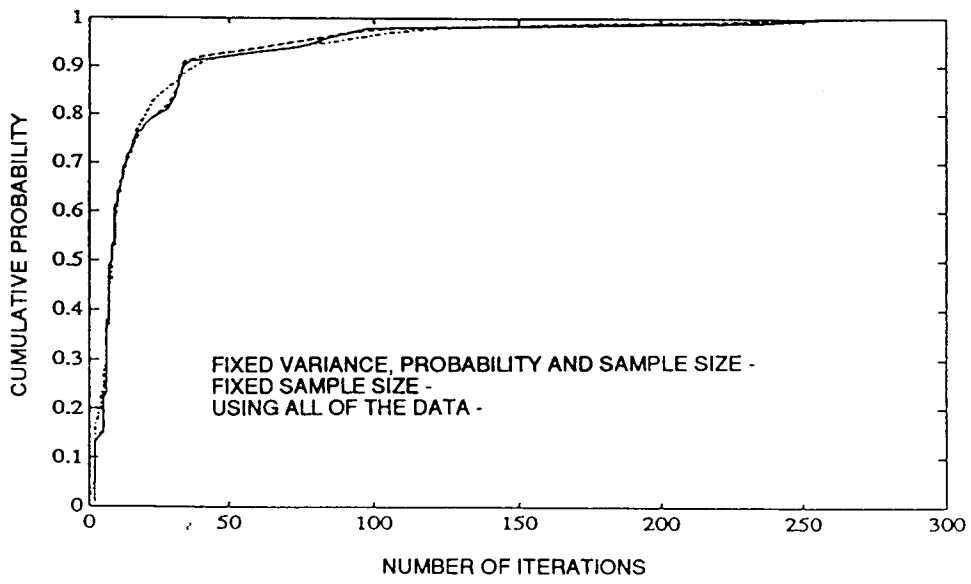

Figure A-4. EM algorithm convergence.

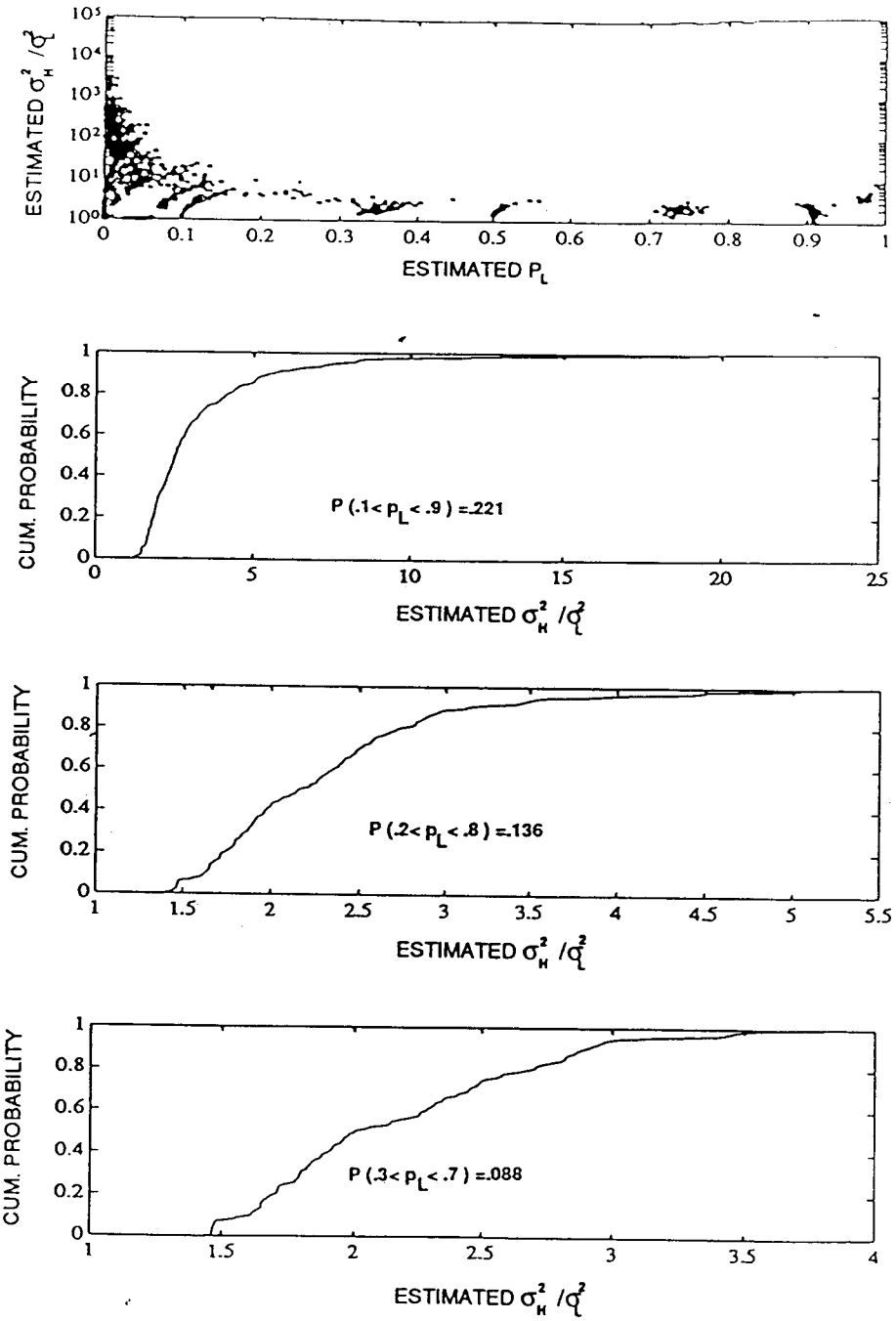

Figure A-5. Two-state mixture model parameter estimates of Gaussian noise and their cumulative probabilities of occurrence.

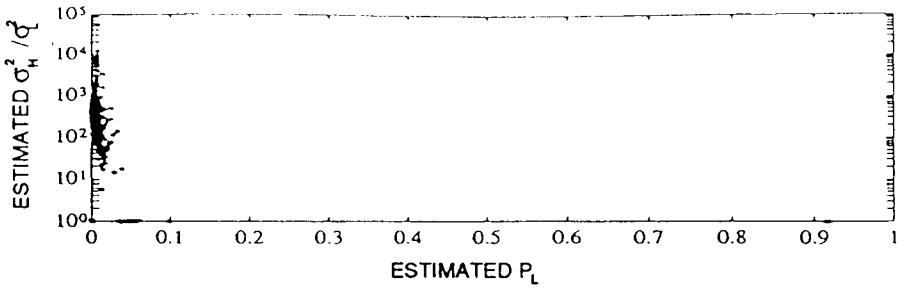

(a) Parameter estimates for SNR = 1.8 dB

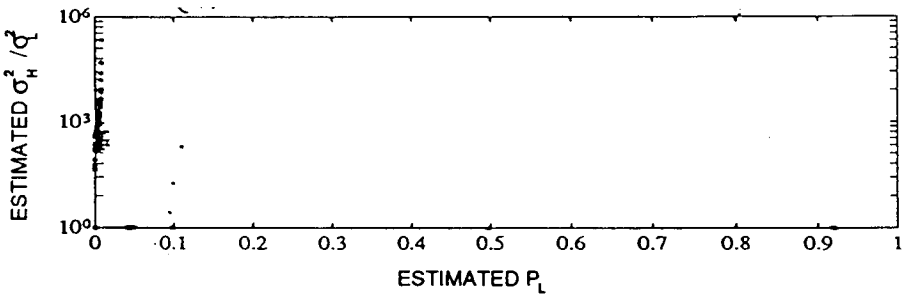

(b) Parameter estimates for SNR = 4.8 dB

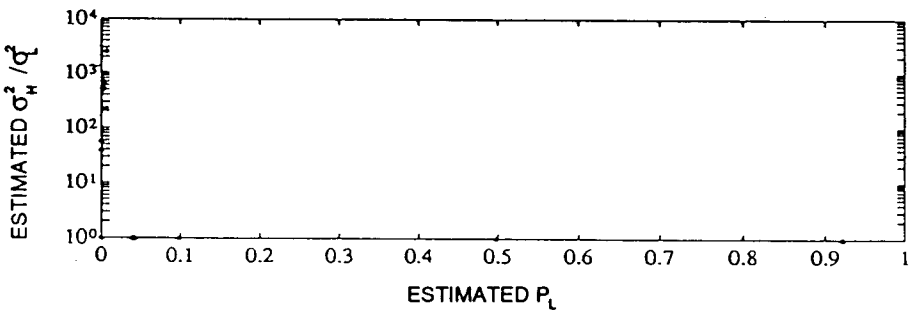

(c) Parameter estimates for SNR = 7.8 dB

Figure A-6. Parameter estimates for the Fourier coefficients of a sinusoid in white Gaussian noise.

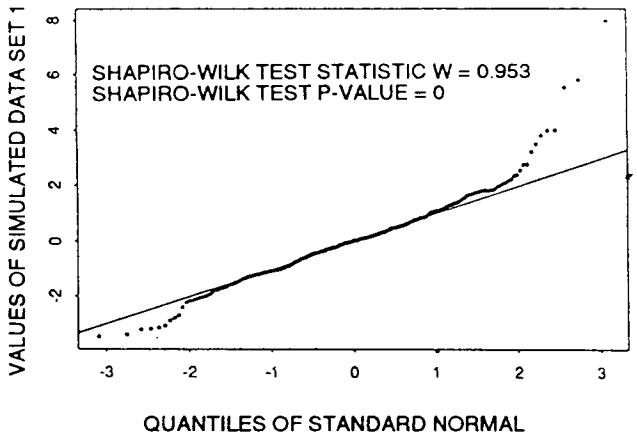

(a) $\sigma_n^2 = 1$, $A = 1$, and $\Gamma = 1$.

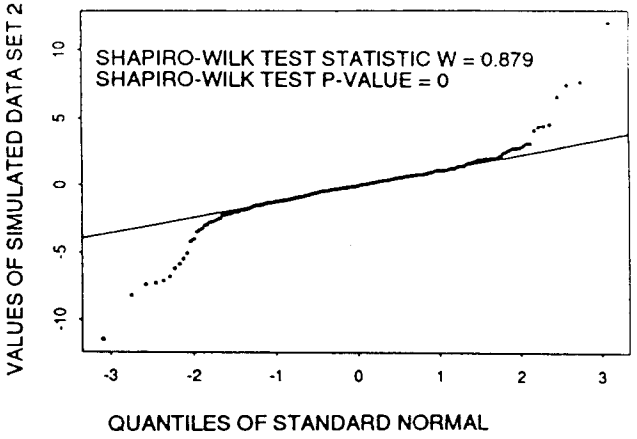

(b) $\sigma_n^2 = 1$, $A = 1$, and $\Gamma = 0.5$.

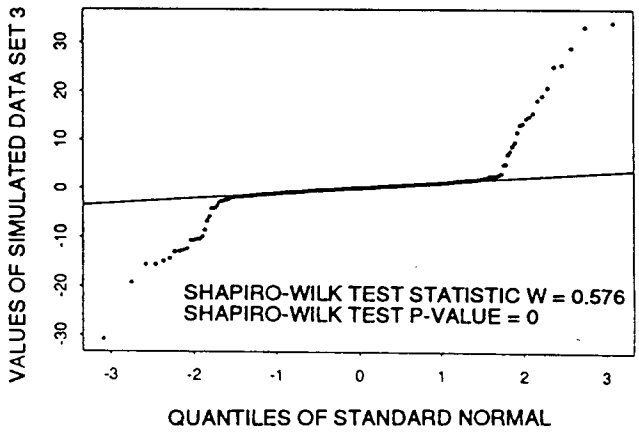

(c) $\sigma_n^2 = 1$, $A = 1$, and $\Gamma = 0.05$.

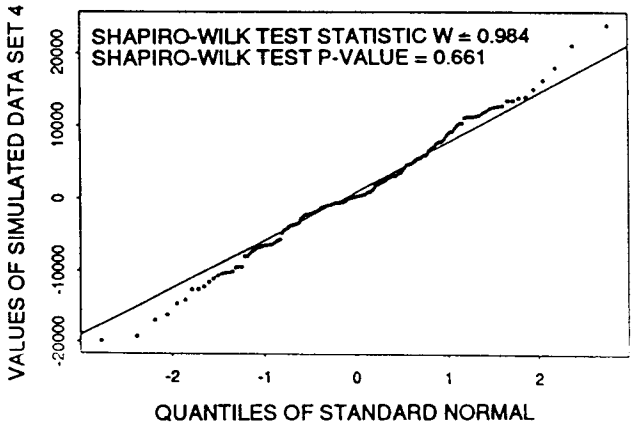

(d) $\sigma_n^2 = 9{,}0000{,}000$, $A = 1.42$, and $\Gamma = 0.127$.

Figure A-7. Normal scores plots for simulated Middleton class A noise.

APPENDIX B
Moving Target Hydrophone Interference Statistics

In this appendix, we present simulation results for a moving target using the Kraken C (Porter, 1992) modal model to calculate the received interference power at a hydrophone. (References in this appendix are listed at the end of the body of this report.) The geometry governing these simulations is that shown in figure 2 of the body of this report for a hydrophone located near the middle of the deep sound channel.

We begin our investigation of the impact of interferer motion on received interferer statistics by examining time series of pressure amplitudes for a 10-meter-deep interference source and for a receiving hydrophone of 800 meters. The interference source is above the deep sound channel and the receiving hydrophone is well within the deep sound channel as can be seen from an examination of figure 3 of the body of the report. The pressure amplitudes are normalized so that 0 dB corresponds to the average received power for the time series of pressure amplitudes for the interferer source at ranges between 10 km and 876 km from a receiving hydrophone at a depth of 800 meters. The results are presented in figure B-1 for four selected range intervals to illustrate the manner in which the fluctuations change as a function of range. The rate and the magnitude of the fluctuations depend on the range of the source. The fluctuations at the hydrophone arise from modes of different wave numbers beating against each other. At longer ranges, the energies in the higher modes are reduced through bottom interaction, as can be seen from an examination of figure B-2, which presents mode amplitudes for the interference source at different ranges from the receiving hydrophone. As a result, fewer modes beat against each other as the range increases and the fluctuations tend to be slower the more distant the interferer from the hydrophone.

Figure B-3 shows the results of the statistical tests and the estimated Gaussian mixture parameters for a source at a depth of 10 meters and the receiving hydrophone at a depth of 800 meters. The amplitude of the pressure data as the source moves from 60 to 375 kilometers was segmented into sets of 128 contiguous samples, representing 27.5 minutes of data for a ship moving at 10 knots, and the sets were overlapped by 50%. The abscissa is the horizontal distance between the hydrophone and the first point of each of the data sets. Figure B-3a presents the significance levels of the Kendall-Mann tau test for the random variable 128-sample average of norms squared and the Kolmogorov-Smirnov two-sample tests for stationarity by comparing the distribution of the first half of the samples with the distribution of the second half of the samples. Figure B-3b shows the significance levels of the Kolmogorov-Smirnov one-sample test for the one-state and the two-state Gaussian mixture model distributions.

The significance levels for the Kolmogorov-Smirnov one-sample test shown in figure B-3b are based on the distribution of the test scores assuming that parameters have not been estimated. The significance levels after adjustment for parameter estimation are lower than those indicated in figure B-3b. However, for the idealized simulation results presented here, it was not deemed necessary to perform a more careful and calculationally demanding statistical analysis of the fit between these data and two-state Gaussian mixture models based on the Cramer-Von Mises and Anderson-Darling goodness-of-fit tests with significance levels adjusted for parameter estimation (Darling, 1955; Stephens, 1974,1976; Sukhatme, 1972).

A two-state Gaussian mixture model is characterized by ratio of its high-state variance σ_H^2 to its low-state variance σ_L^2 and its low-state probability p_L and these are the estimated parameters for the two-state Gaussian mixture model plotted in figures B-3c and d. Note that the ratio of high-state to low-state variance is plotted in figure B-3c on a log base 2 scale. The joint probability density function for the low-state probability and the ratio of high-state to low-state variance is shown for the estimates for two-state Gaussian mixture parameter for a moving interferer in 10 kilometer steps from 350 to 500 kilometers. The selected data span a convergence zone located at 372 kilometers.

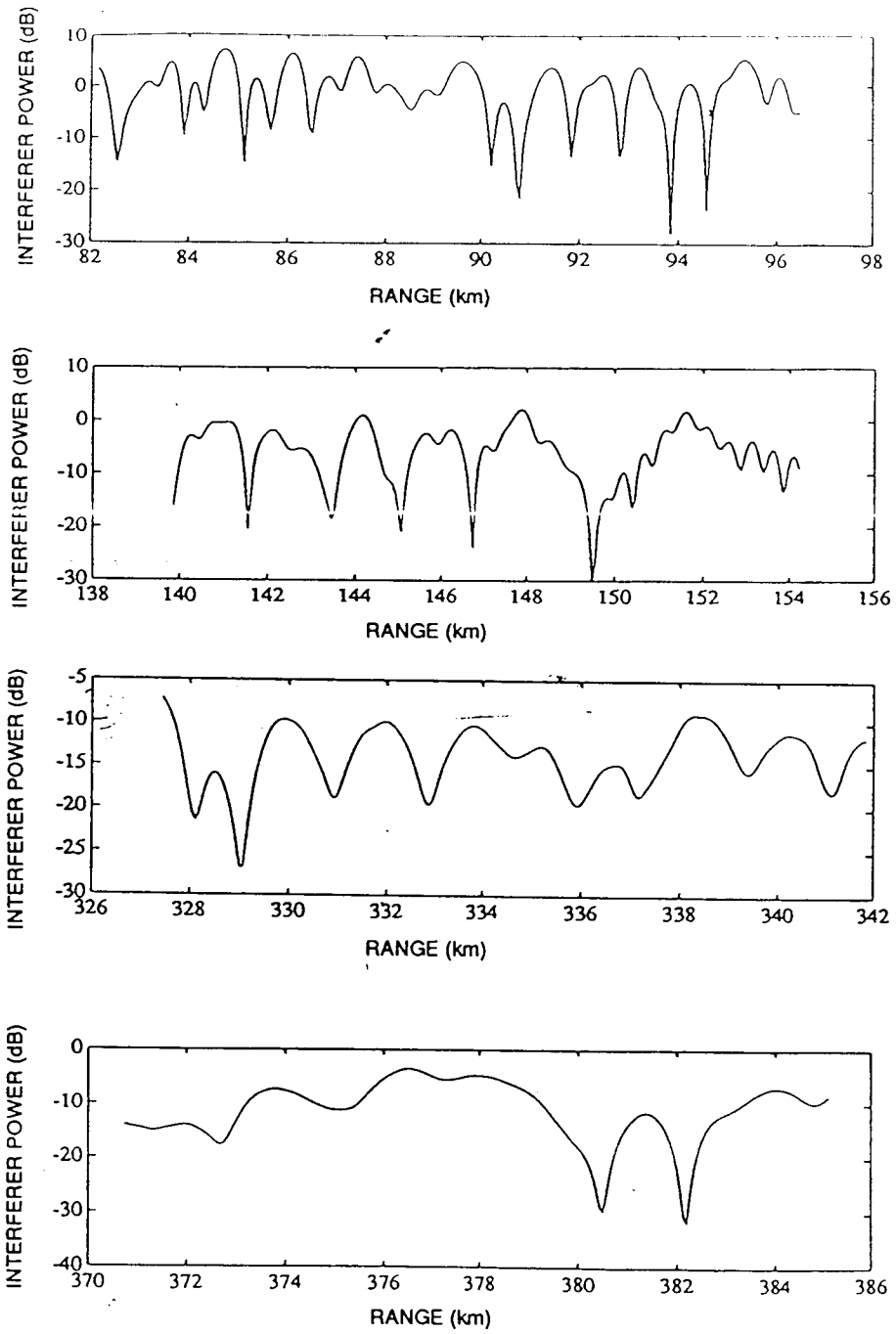

Figure B-1. Predicted interferer power as a function of range to a receiving hydrophone.

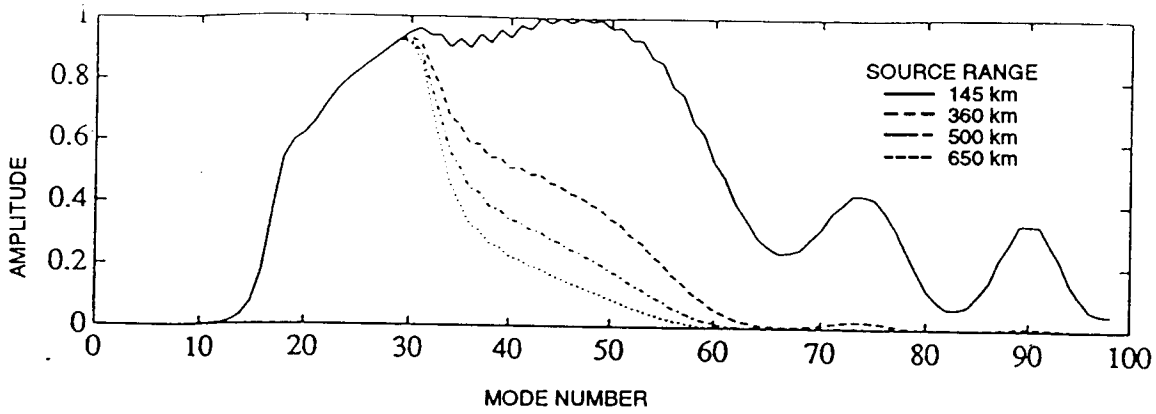

Figure B-2. Propagation mode amplitude.

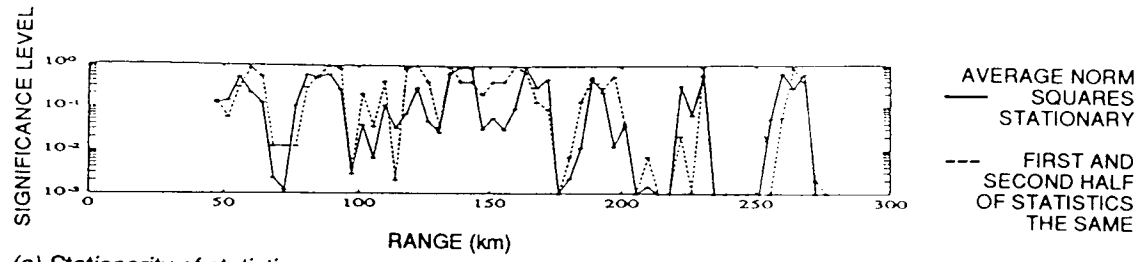

(a) Stationarity of statistics.

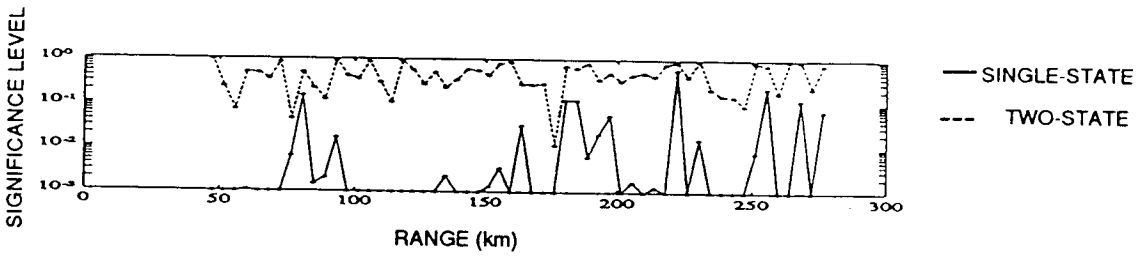

(b) Nature of model.

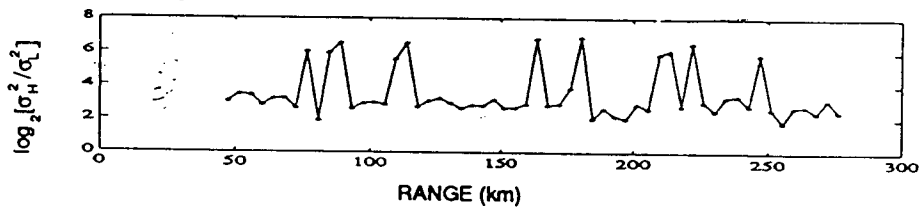

(c) Variance ratio estimates for R-state model.

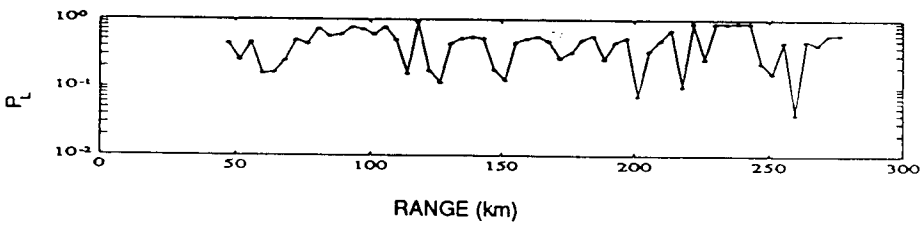

(d) Low-state probability estimates for two-state model.

Figure B-3. Interferer statistics as a function of range from a moving source and receiving hydrophone.

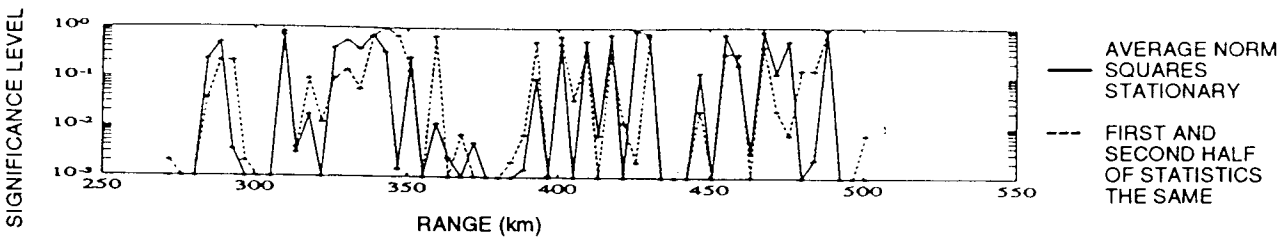

(a) Stationarity of statistics

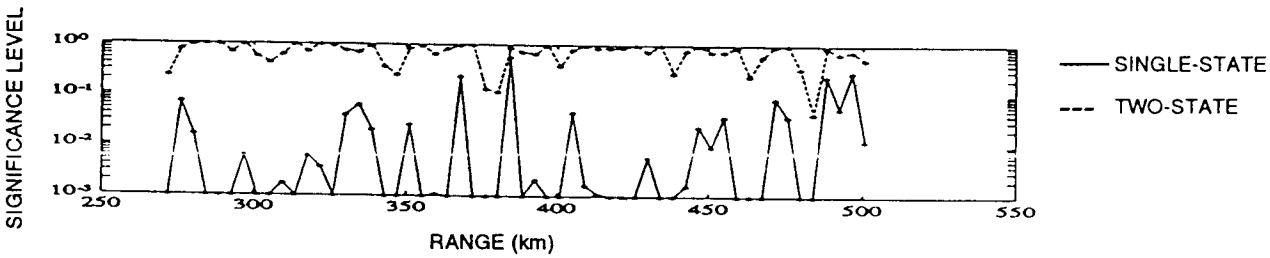

(b) Nature of model

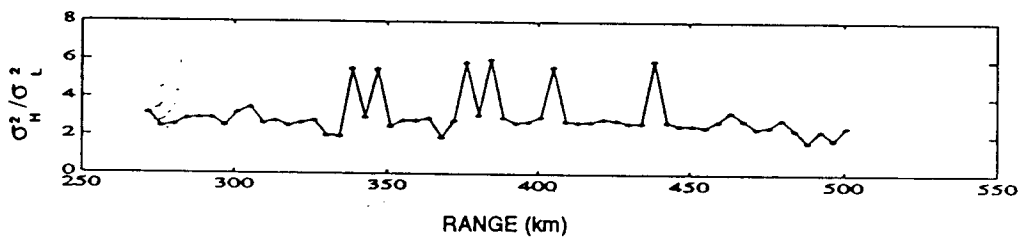

(c) Variance ratio estimates for R-state model

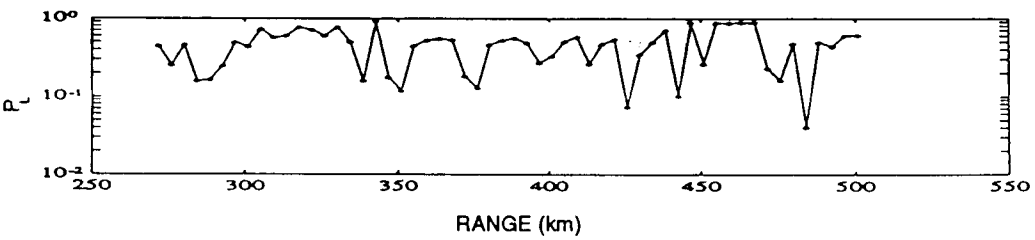

(d) Low-state probability estimates for two-state model

Figure B-3 Interferer statistics as a function of range from a moving source and receiving hydrophone (continued).

A single two-state mixture model with parameters $p_L = 0.5$ and variance ratio between 4 and 8 provides a good fit to most of the selected hydrophone data as shown in figure B-4. A second two-state mixture model occurs around 10% of the time with a high-state to low-state variance ratio exceeding 32. Figure B-3c indicates that the higher variance ratio mixture model applies to at most two successive samples, that to a period of time roughly corresponding to the period of time required for the interferer to move 12 kilometers toward the receiving hydrophone.

Figure B-3a suggests that the amplitude fluctuations at the hydrophone output caused by the source motion can often be better described by a two-state Gaussian mixture model than by a one-state model. However, the ratio of high-state to low-state variance is only 6 dB for the most commonly occurring mixture model.

The simulated hydrophone data were also compared to the three-state model with parameters obtained using the EM model. The initial parameter vectors were obtained from the best estimate of the two-state parameters for the data being fit as described in appendix A. The time histories of the three-state levels of significance exhibited similar properties to those exhibited for the two-state time histories of levels of significance so that these histories are not presented. Instead, we focus on comparing the significant levels for comparisons of the data with one-state, two-state, and three-state Gaussian mixture models and determining the L2 norms of the differences between the one-state and the two-state fits, the one-state and the three-state fits, and the two-state and three-state fits to the data. Recall that for two vectors $x = (x_1, x_2, ..., x_n)$ and $y = (y_1, y_2, ..., y_n)$, the L2 norm of the difference is simply the Euclidean distance $||x-y||_2 = \sqrt{\sum_{i=1}^{n}(x_i - y_i)^2}$.

Histograms of the significant levels for the Chi-squared test and the Kolomogorov-Smirnov one-sample test comparing the empirical data with one-state, two-state, and three-state Gaussian mixture models are presented in figures B-5 and B-6, respectively. The relationship between levels of significance and test scores differ for the three cases as shown in figure B-6. The different relationships occur because the number of degrees of freedom for the Chi-squared test depends on the number of states for the mixture model, 23 for a one-state model, 21 for a two-state model, and 19 for a three-state model. The Chi-squared test significant levels tend to be very low (left-most bin shown in figure B-5) nearly 80% of the time for a one-state model, 17% of the time for a two-state model, and 1% for a three-state model. Thus either a two-state or three-state model fits nearly all the data better than a one-state as already discussed, while some of the time a three-state model fits the data better than either a one-state or a two-state model. Figure B-7 presents a histogram of the L2 norms of the differences between the models obtained that best fit the data. This data shows that more than 80 percent of the time, the two-state and three-state fits lead to nearly the same probability density functions.

Figure B-8 summarizes the probabilities of occurrence of the three-state model parameters $p_L, p_M, p_H, \frac{\sigma_M^2}{\sigma_L^2}, \frac{\sigma_H^2}{\sigma_L^2}$, obtained using the EM algorithm for the hydrophone data. A few three-state models do not predominate the three-state models that best fit the hydrophone data, unlike for the two-state models. The surprising result is the high percentage of cases in which the best three-state model probability was between 0.4 and 0.6 as shown in figure B-8b. This means that a large percentage of samples formerly in the low and high states fall into the middle state, while the middle-state to low-state variance clustered about 3 and the high-state to low-state variance about 6, so that the dynamic range as measured by the difference between the variances of the low and high states did not dramatically increase when the data was fit by a three-state model from when it was fit by a two-state model.

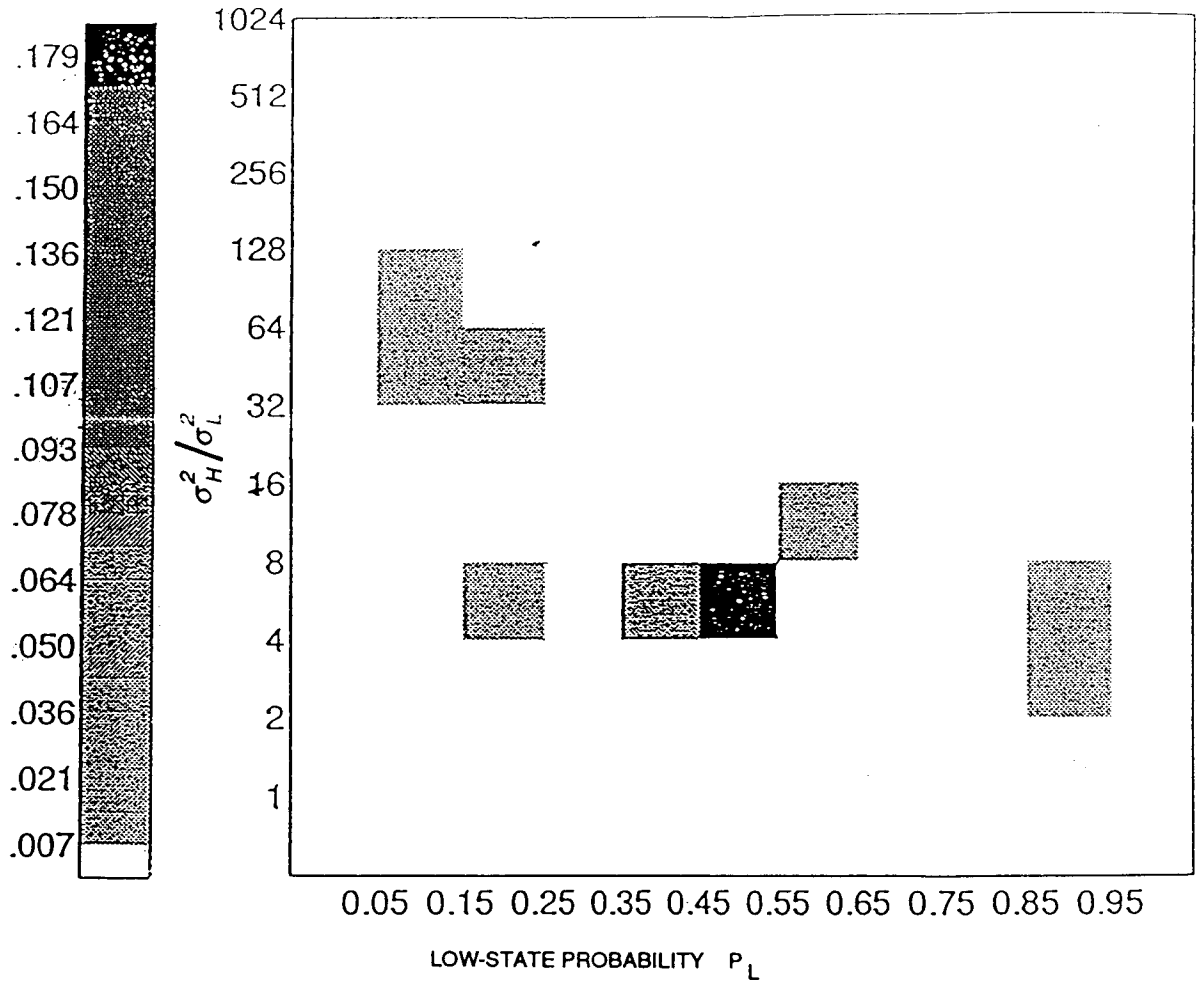

Figure B-4. Joint probability density function of low-state probability and state variance ration for simulated hydrophone data near a convergence zone.

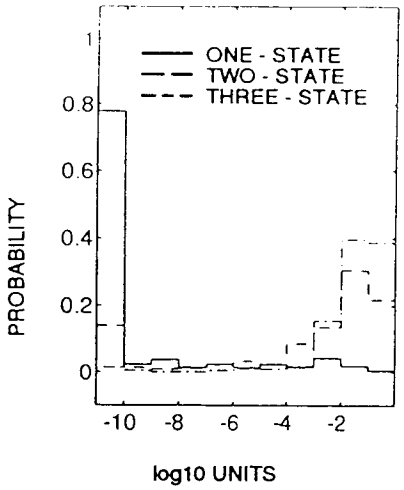

Figure B-5. Mixture model Chi-squared test significance levels for hydrophone data.

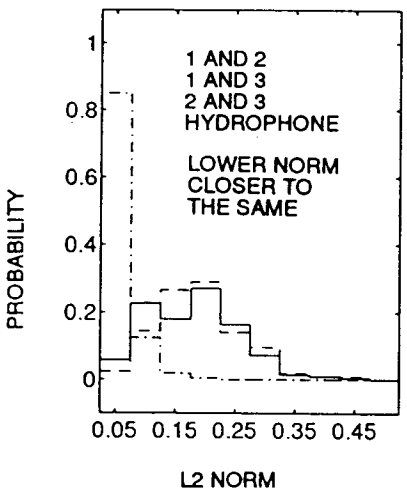

Figure B-7. Differences between mixture model probability densities for hydrophone data.

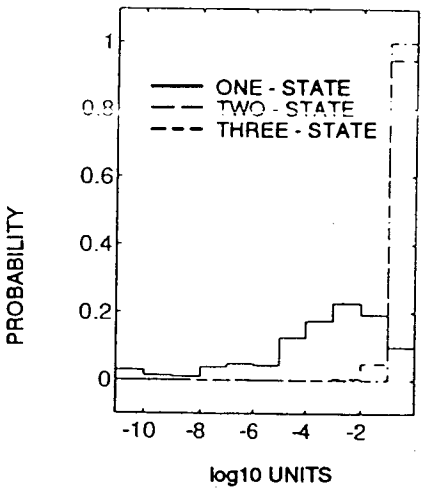

Figure B-6. Mixture model Kolmogorov-Smirnov one-sample test significance levels for hydrophone data.

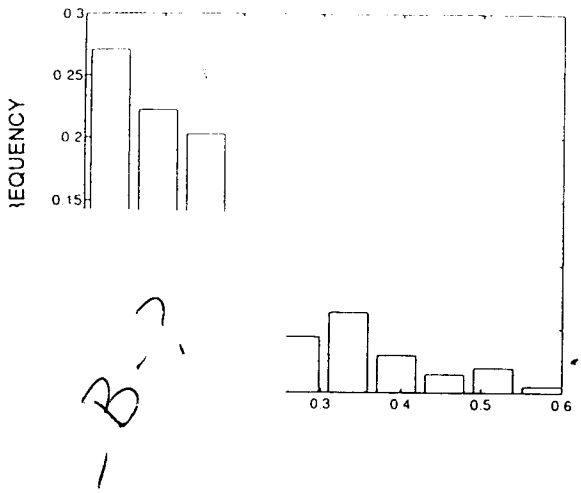

Figure C-8. Three-state parameter distributions for hydrophone data.

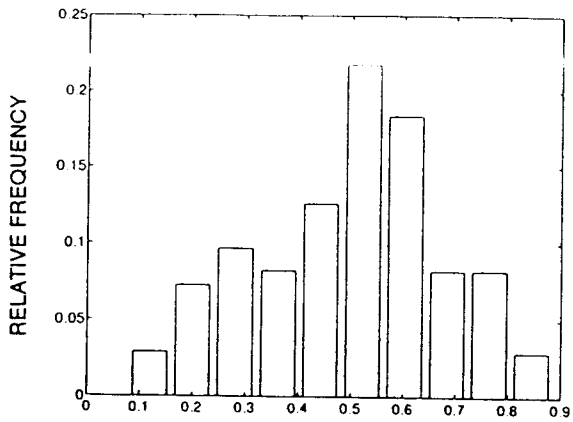

(b) Middle-state probability

Figure B-8. (Con't.) Three-state parameter distributions for hydrophone data.

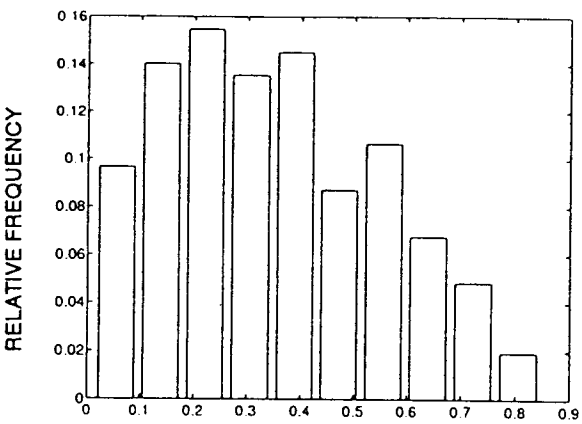

(c) High-state probability

Figure B-8. (Con't.) Three-state parameter distributions for hydrophone data.

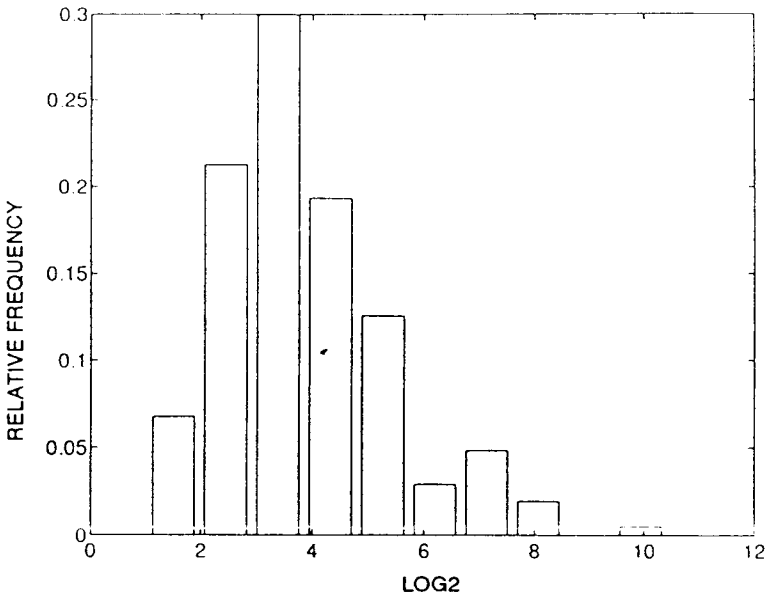

(d) Middle-state to low-state variance

Figure B-8. (Con't.) *Three-state parameter distributions for hydrophone data.*

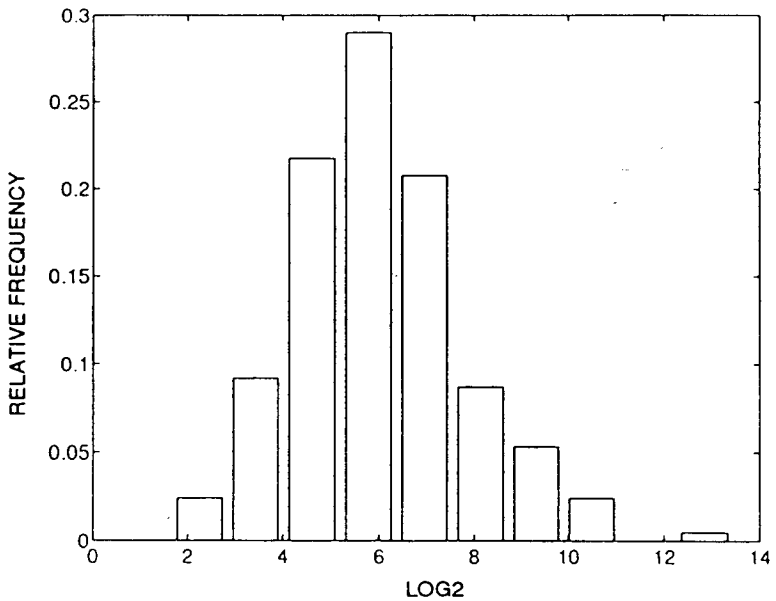

(e) High-state to low-state variance

Figure B-8. (Con't.) *Three-state parameter distributions for hydrophone data.*